AIMS Materials Science, 12(3): 562–609.
DOI: 10.3934/matersci.2025025
Received: 08 April 2025
Revised: 05 June 2025
Accepted: 13 June 2025
Published: 02 July 2025

http://www.aimspress.com/journal/Materials

Review

Applications of piezoelectric and biomedical metamaterials: A review

Qinghua Qin*

Institute of Advanced Interdisciplinary Technology, Shenzhen MSU-BIT University, Shenzhen 518172, China

* **Correspondence:** Email: qinghua.qin@smbu.edu.cn; Tel: +86-755-28323312.

Abstract: In this review, we provide a comprehensive overview of recent advances in bioinspired and piezoelectric metamaterials, focusing on their applications in biomedical engineering, smart sensing, and related fields. We examined how artificially engineered micro- and nanostructures enable metamaterial-based biosensors to achieve highly sensitive, label-free detection of biomolecules across microwave, terahertz, and optical frequencies, with detection limits reaching the attomolar level. These capabilities offer transformative potential for cancer biomarker screening, rapid viral diagnostics, and cellular activity monitoring. We also highlight the growing role of piezoelectric metamaterials in structural health monitoring, including low-frequency vibration suppression and acoustic wave control, as well as in biomedical applications such as bone tissue regeneration and self-powered medical devices, enabled by advances in electromechanical coupling and structural design. In addition, the integration of bioinspired architectures with 3D printing has led to the development of multifunctional metamaterials exhibiting features such as negative Poisson's ratios and adaptive mechanical responses, with promising applications in soft robotics, tissue scaffolds, and protective systems. We further discussed terahertz metamaterial devices, including perfect absorbers, polarization converters, and smart sensing platforms that incorporate microfluidics and plasmonic resonance, driving innovation in precision medicine and environmental monitoring. Collectively, these developments emphasize the importance of a "structure–function–intelligence" design paradigm and offer strategic insights into emerging research directions across healthcare, communications, and aerospace. We conclude by summarizing key analytical and fabrication methodologies, referencing 193 scholarly works.

Keywords: metamaterials; biomedical applications; negative Poisson's ratio; terahertz sensing; piezoelectric effect; tissue engineering

1. Introduction

Metamaterials are an emerging class of functional materials defined by artificially engineered subwavelength architectures (see Figure 1), where the physical properties are governed more by structure than composition [1–4]. Through innovative geometrical and structural design [5–8], metamaterials can exhibit exceptional properties not found in natural materials, such as negative refractive index, negative Poisson's ratio, unconventional acoustic responses, and extreme mechanical behaviors. Recent advances in additive manufacturing, micro/nanofabrication, and computational modeling have significantly broadened the scope of metamaterial research, from its origins in electromagnetic manipulation to a wide array of domains including mechanics, acoustics, thermal regulation, and biomedicine, underscoring their growing potential in real-world applications.

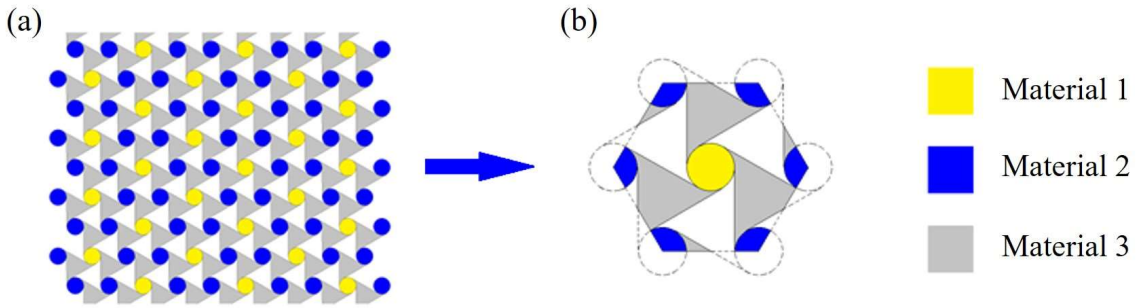

Figure 1. Schematic of an artificial chiral metacomposite with periodic cells. (a) Composite with periodic cells; (b) meta-unit cell. The composite contains three materials with different mechanical/physical properties. The degenerated case is all three materials becoming identical.

In the biomedical field, metamaterials have driven transformative advancements in tissue engineering, diagnostics, and therapeutics, thanks to their customizable architectures and multifunctional capabilities. For instance, auxetic metamaterials, which expand laterally when stretched, exhibit mechanical behavior that closely aligns with human bone, making them promising candidates for bone repair implants [9–11]. Specifically, their unique deformation behavior offers key advantages: (1) a Poisson's ratio comparable to that of bone and (2) enhanced energy absorption and fracture resistance, as the densification under compression improves impact tolerance, much like how bone absorbs shocks during walking or running. These properties make auxetic metamaterials ideal for mimicking bone mechanics, improving load sharing, and reducing stress shielding, all critical factors for long-term implant performance. Additionally, terahertz (THz) metamaterial biosensors enable label-free, highly sensitive detection for early-stage cancer diagnostics [12,13], viral identification [14], and real-time monitoring of biomolecular interactions [15]. Moreover, piezoelectric metamaterials, which transduce mechanical stimuli into electrical signals, are paving the way for self-powered biomedical devices, including cochlear implants [16] and mimicking biomaterials [17,18]. Furthermore, bioinspired metamaterials, which integrate biomimetic principles with engineered architectures, are emerging as intelligent materials across materials science, engineering, and biomedicine [19–21]. By mimicking natural structures, these materials offer enhanced mechanical resilience, optical tunability, antifouling performance, and energy harvesting capabilities, delivering innovative solutions to complex biomedical and engineering challenges.

Despite substantial progress, several challenges persist in the design, fabrication, and clinical translation of biomedical metamaterials. Key issues include:

- Balancing mechanical performance with biological function through multiscale structural optimization [22,23].
- Enhancing sensor specificity and resistance to environmental or biochemical interference [24,25].
- Addressing biocompatibility-performance trade-offs or enhancing patient care in piezoelectric systems [26,27].

Moreover, interdisciplinary collaboration and the development of standardized evaluation frameworks are essential to advance these technologies from laboratory prototypes to clinical and industrial applications.

To provide conceptual clarity and guide readers through the diverse landscape of metamaterials discussed in this review, we offer the following definitional framework outlining the scope and distinguishing characteristics of each major category:

(1) Piezoelectric metamaterials (Section 3):

Architected materials that incorporate piezoelectric effects, where mechanical stress induces electrical charge and vice versa, into metamaterial structures. These systems are primarily explored for wave manipulation, electromechanical coupling, and vibration control, enabled by tailored geometries and material heterogeneity.

(2) Metamaterial-based biosensors (Section 4):

Functional devices leveraging the electromagnetic resonance properties of metamaterials for high-sensitivity, label-free detection of biological entities (e.g., molecules, cells and pathogens). Applications include medical diagnostics, environmental monitoring, and point-of-care systems.

(3) Bioinspired metamaterials (Section 5):

Materials whose designs are informed by natural structures or biological processes (e.g., nacre, bone, and skin). While not always biomedical in application, their architectures achieve enhanced mechanical, acoustic, or multifunctional properties by mimicking evolutionary strategies.

(4) Biometamaterials (Section 6):

Metamaterials engineered to interact with biological systems, including tissue scaffolds, orthopedic implants, and materials, offering mechanical compatibility with living tissues. While often inspired by nature, their defining feature lies in their targeted biomedical function than their geometric resemblance to biological forms.

By delineating these categories, we aim to enhance the coherence of the review, clarify the unique contributions of each metamaterial class, and highlight their respective roles in advancing biomedical and multifunctional material technologies.

2. Basic approaches for metamaterial analysis

In this section, we introduce several key preliminary concepts, focusing on meta-unit design, model development, and analytical methodologies. The following discussion draws primarily on the work of Wang et al. [28], Hu et al. [29], Aghighi et al. [30] and Dong et al. [6]. For a comprehensive overview of the procedures applicable to both 2D and 3D periodic materials, readers are referred to [31].

2.1. A meta unit composed of periodic spindle-shaped plumbum inclusions in a rubber matrix

In this subsection, we present a meta-unit exhibiting a complete bandgap at low frequencies. The design consists of spindle-shaped or S-shaped inclusions periodically embedded within a rubber matrix, with their axes oriented parallel to the crystal surfaces [28,32]. Using the finite element method (FEM) in combination with Bloch's theorem [33], we analyze the wave propagation characteristics, including dispersion relations, transmission spectrum, effective mass, and displacement fields.

2.1.1. Meta-unit and finite element formulation

As an illustration, Figure 2a,b present schematic diagrams of the cross-section of the proposed phononic crystal structure and its representative unit cell, respectively [32]. The geometric parameters of the unit cell, including the S-shaped slot, are defined as follows: a represents the lattice constant of the square unit cell, while m and n denote the vertical dimensions indicated in Figure 1b. The horizontal length of the S-shaped slot is designated as *l*, and the slot width is denoted by *d*. The structure is considered to be infinite along the z-axis, justifying the use of a plane strain assumption in the subsequent analysis.

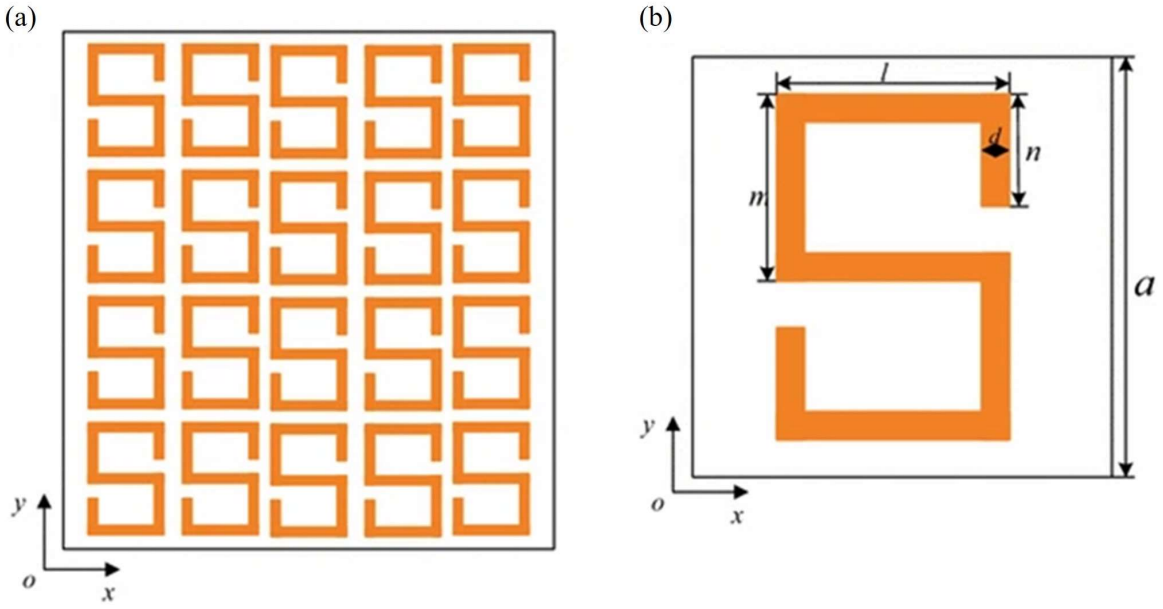

Figure 2. (a) Schematic view of the cross-section of the two-dimensional phononic crystal. (b) The representative unit cell of the proposed phononic crystal (Reproduced from Ref. [32] with permission).

The governing Eq 1 is for elastic wave propagation in homogeneous solids [28]:

$$\sum \sum_{j=1}^{3} \frac{\partial}{\partial x_j} \left(\sum_{l=1}^{3} \sum_{k=1}^{3} c_{ijkl} \frac{\partial u_k}{\partial x_l} \right) = \rho \frac{\partial^2 u_i}{\partial t^2} \ (\mathrm{i} = 1,2,3) \tag{1}$$

where ρ is the mass density, t is the time, u_i is the i-th component of the displacement vector $u(r)$ with position vector r, c_{ijkl} are the elastic constants, and x_j (j = 1,2,3) are the corresponding coordinate variables x, y, and z, respectively.

The dispersion diagram (or band structure) of a metamaterial illustrates the relationship between the frequency (ω) and wave vector (k) of propagating waves, revealing properties like bandgaps, anisotropy, and wave steering effects. Below is the standard method and key equations for computing dispersion diagrams in periodic metamaterials.

For a periodic meta-unit system, wave propagation is governed by Bloch's theorem (Eq 2), which states that the solution $u(r,t)$ (displacement, electric field, etc.) can be expressed as:

$$\mathrm{u}(r,t) = e^{i(k\cdot r-\omega t)}\mathrm{U}_k(r) \tag{2}$$

where $U_k(r)$ is a periodic vector with the same periodicity as the crystal lattice (meta-unit system), $i = (-1)^{1/2}$, r is the position vector, and $k = (k_x,k_y)$ is the wave vector limited to the first Brillouin zone of the repeated lattice.

The governing equation, whether mechanical, electromagnetic, or acoustic, reduces to an eigenvalue problem in the frequency domain. For instance, in periodic elastic metamaterials (mechanical waves), the wave equation (Eq 3) can be expressed as:

$$\nabla \cdot (C(r):\nabla u) = -\rho(r)\omega^2 u \tag{3}$$

where C is the stiffness tensor and ρ is the mass density.

By applying Bloch's theorem to this wave equation, it is transformed into the following eigenvalue problem:

$$L(k)U_k = \omega^2 U_k \tag{4}$$

where L is a Hermitian operator dependent on k. Solving this equation yields the dispersion relation $\omega_n(k)$ for each band n.

Using the finite element method (FEM), the discrete form of the eigenvalue Eq 4 within the representative unit cell can be written as:

$$(K - \omega^2 M)U = 0 \tag{5}$$

In Eq 5, U the displacement vector at the discrete node, K and M are the stiffness and mass matrices of the meta-unit cell, respectively, and ω is the circular frequency.

Considering the periodicity of the structure, the following Bloch periodic boundary condition (Eq 6) should be applied to the meta-unit cell based on the Bloch theorem:

$$u(r + a) = u(r)e^{ik\cdot a} \tag{6}$$

where $a = (a_x,a_y)$ is the lattice basis vector, with $a_x = a_y = a$.

After a series of numerical simulations with FEM [28], the corresponding transmitted displacement can be recorded on the right boundary of the output domain to evaluate the transmission spectrum defined as follows [28]:

$$TL = 10\,log_{10}\left(\frac{u_{in}}{u_{out}}\right) \tag{7}$$

In Eq 7, u_{in} and u_{out} are the values of the incident displacement and transmitted displacement, respectively. By varying the excitation frequency of the incident displacement, the transmission spectrum can be obtained.

The solution outlined above is summarized below in a step-by-step format:

Step 1: define the unit cell—Specify the geometry and material properties (e.g., density ρ and stiffness C).

Step 2: discretize the Brillouin zone—Trace the wave vector (k) paths along high-symmetry points (e.g., Γ–X–M–Γ for square lattices).

Step 3: solve the eigenvalue problem—For each k, numerically compute the eigenfrequencies $\omega_n(k)$.

Step 4: post-processing—Plot ω versus k and identify bandgaps (frequency ranges where no real ω exists).

2.1.2. Effective mass density of the meta-unit

If the periodic model is treated as an equivalent elastic solid, the effective material parameters based on the homogenization concept can be used to characterize the properties of the meta-unit. The average of local fields, including the local stress $\sigma_{\alpha\beta}$, strain $\varepsilon_{\alpha\beta}$, forces F_α, and displacement u_α, is imposed on the external boundary of the representative volume element as [28]:

$$\tilde{\sigma}_{\alpha\beta} = \frac{1}{V}\int_{\partial V} \sigma_{\alpha\lambda} x_\beta \, ds_\lambda;\ \tilde{\varepsilon}_{\alpha\beta} = \frac{1}{V}\int_{\partial V} (u_\alpha \, ds_\beta + u_\beta ds_\alpha)$$
$$F_\alpha = \int_{\partial V} \sigma_{\alpha\lambda} \, ds_\lambda;\ \tilde{\ddot{u}}_\alpha = \frac{1}{S}\int_{\partial V} -\omega^2 u_\alpha \, ds \tag{8}$$

In Eq 8, the over-bending line is the average field. The meta-unit used in [28] is a two-dimensional system, and the constitutive equation in principal axes can be expressed as:

$$\begin{Bmatrix} \tilde{\sigma}_{11} \\ \tilde{\sigma}_{22} \\ \tilde{\sigma}_{12} \end{Bmatrix} = \begin{bmatrix} c_{11}^{eff} & c_{12}^{eff} & 0 \\ c_{12}^{eff} & c_{11}^{eff} & 0 \\ 0 & 0 & c_{44}^{eff} \end{bmatrix} \begin{Bmatrix} \tilde{\varepsilon}_{11} \\ \tilde{\varepsilon}_{22} \\ 2\tilde{\varepsilon}_{12} \end{Bmatrix} \tag{9}$$

In Eq 9, $\tilde{\varepsilon}_{\alpha\beta} = (\tilde{u}_{\alpha,\beta} + \tilde{u}_{\beta,\alpha})/2$, for $\alpha,\beta = 1,2$ and $c_{\alpha\beta}^{eff}$ representing the effective stiffness tensor. Based on the average fields, the equation of motion (Eq 10) is written as:

$$\frac{\partial \tilde{\sigma}_{\alpha\beta}}{\partial x_\beta} = \rho_{eff} \frac{\partial^2 \tilde{u}_\alpha}{\partial t^2} \tag{10}$$

where ρ_{eff} is effective mass density, which can be calculated from Newton's second law (Eq 11) as follows:

$$\rho_{eff} = \frac{F_\alpha}{V\ddot{u}_\alpha} = \frac{F_\alpha}{-V\omega^2 u_\alpha} \tag{11}$$

2.2. A chiral auxetic metamaterial unit cell generated from a polynomial

In [6], the following polynomial is utilized to generate a chiral auxetic metamaterial unit cell. The polynomial expression is given as:

$$\frac{y-y_A}{y_B-y_A} = \left(\frac{x-x_A}{x_B-x_A}\right)^n \text{ and } \frac{y-y_C}{y_D-y_C} = \left(\frac{x-x_C}{x_D-x_C}\right)^n \tag{12}$$

In Eq 12, points *A*, *B*, *C*, and *D* are shown in Figure 3. It is important to note that the structure considered here consists of identical repeating unit cells arranged in translational symmetry. Each unit cell comprises four branches connected at its center, exhibiting rotational symmetry. The auxetic sample with the chiral pattern is shown in Figure 3c, where the entire structure consists of a 6 × 6 array of the four-pronged unit cells, each rotated 45° around its center.

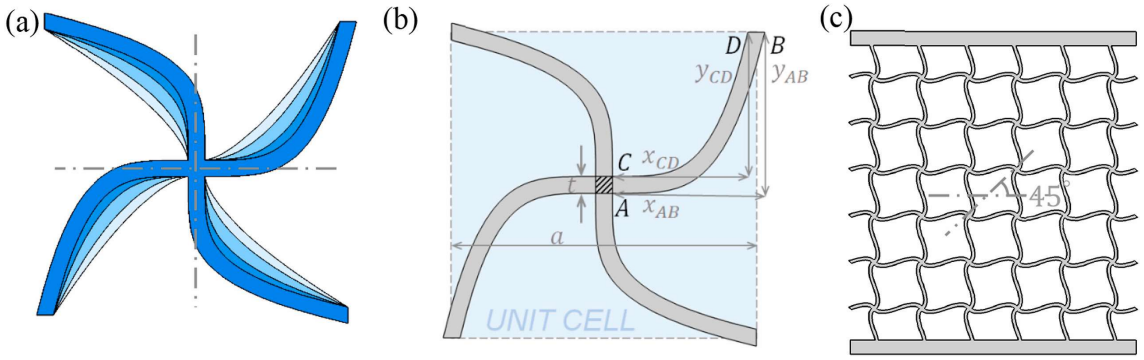

Figure 3. Design of the chiral pattern: (a) unit cell variations at n = 1.5, 2, 3, and 4; (b) shape parameters defining the geometry of the unit cell; and (c) the 6 × 6 test sample consisting of repeating units that are rotated 45° around the center (Reproduced from Ref. [29] with permission).

To construct a cross-chiral lattice, Dong et al. [6] incorporated both the original unit cell topology and its mirrored counterpart. Using the polynomial framework described in [29], a cross-chiral lattice can be readily generated, as illustrated in Figure 4a. Each unit cell, highlighted in the figure, consists of a central joint and four curved, rotating ribs positioned at 90° intervals. Figure 4b provides a detailed view of the rib's parameterized curvature. The rib's centerline is defined by a cubic interpolation spline passing through three control points, A, B, and C. A rib is then formed by sweeping a uniform rectangular cross-section along this centerline. Figure 4c illustrates the deformation mechanism of the cross-chiral metamaterial structure (CMS) unit cell under uniaxial tension in the x-direction, which is used to evaluate mechanical performance. When longitudinal tension is applied, the central joint undergoes rotation and the curved ribs unwind, resulting in transverse expansion of the unit cell.

This lateral expansion is characterized by a negative Poisson's ratio. In this work, the negative Poisson's ratio is calculated as follows [6]:

$$\varepsilon_x = \frac{\Delta X}{X} = \frac{(\Delta x_2+\Delta x_4)/2-(\Delta x_1+\Delta x_3)/2}{a} \tag{13}$$

$$\varepsilon_y = \frac{\Delta Y}{Y} = \frac{(\Delta y_3+\Delta y_4)/2-(\Delta y_1+\Delta y_2)/2}{a} \tag{14}$$

$$\nu_{yx}(t) = -\frac{\varepsilon_x}{\varepsilon_y} \tag{15}$$

In Eqs 13–15, *x* and *y* displacement measurements are retrieved from probing points 1, 2, 3, and 4, as illustrated in Figure 4.

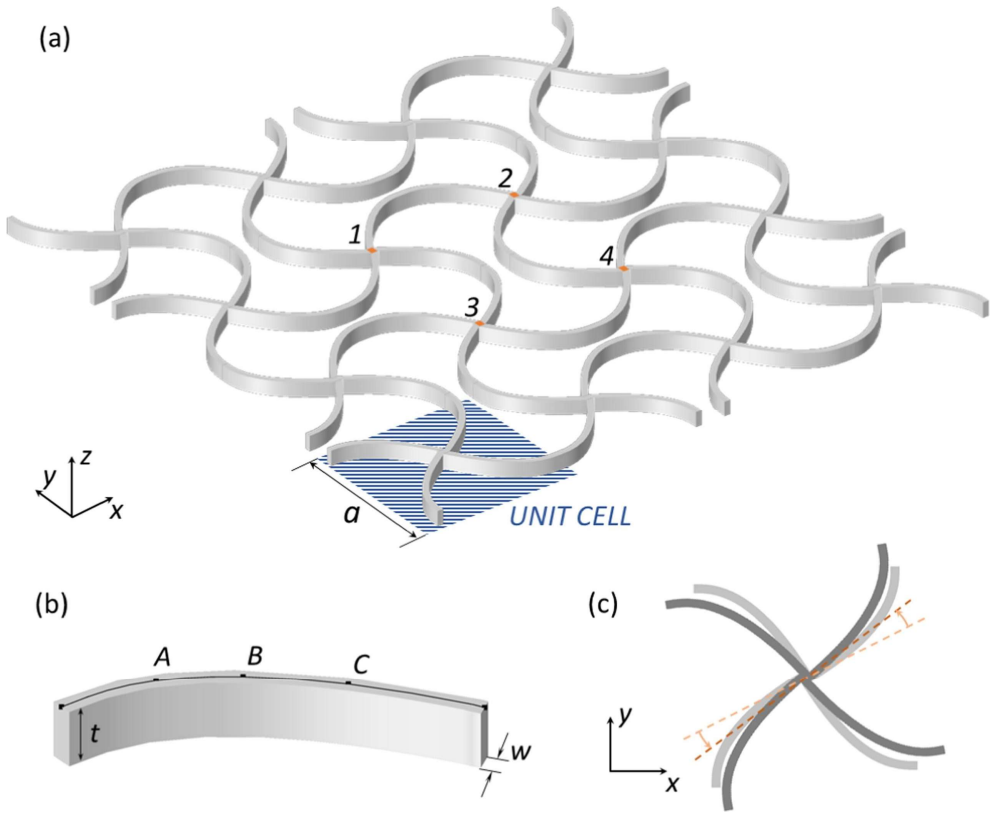

Figure 4. (a) Schematic of the cross-chiral metamaterial structure (CMS). (b) Curved rib with parameterized curvature. (c) Deformation mechanism of the CMS unit cell (Reproduced from Ref. [6] with permission).

2.3. Numerical modeling in periodic metamaterial systems: Focus on finite element analysis (FEA) and Bloch's theorem

FEA and Bloch's theorem constitute foundational tools in the numerical modeling of periodic metamaterial systems. FEA enables the discretization of complex unit-cell geometries and the solution of governing partial differential equations under appropriate boundary conditions, facilitating detailed simulations of elastic wave propagation, mode shapes, and localized resonances. Bloch's theorem, by exploiting spatial periodicity, simplifies the modeling of infinite structures by reducing the problem to a single representative unit cell. Within this framework, wave behavior is captured through eigenvalue problems across the first Brillouin zone. When integrated with FEA, Bloch-periodic conditions enable efficient and accurate computation of dispersion relations and bandgap characteristics. However, the fidelity of these simulations depends critically on the precise treatment of internal interface conditions.

2.3.1. Bloch's theorem in periodic systems

Originating from solid-state physics, Bloch's theorem states that wave solutions in periodic media can be expressed as a plane wave modulated by a periodic function (Eq 6). This enables the reduction of an infinite periodic structure to a finite unit cell with phase-shifted boundary conditions. By transforming wave propagation problems into eigenvalue formulations, either for frequency at a given wavenumber or vice versa, this approach significantly reduces computational cost. It is widely used to

determine band structures (dispersion relations) and identify phononic or photonic bandgaps, which are essential for designing metamaterials with targeted wave-filtering, guiding, or attenuation capabilities.

2.3.2. Coupling FEA with Bloch boundary conditions

In practical implementations, the representative unit cell is meshed using finite elements, and Bloch-periodic boundary conditions (Eq 16) are applied to opposing faces to enforce periodicity:

$$u(x + a) = u(x)e^{ik \cdot a} \tag{16}$$

This transforms the governing equations into a parametric eigenvalue problem, where the wave vector k is swept through the irreducible Brillouin zone. The resulting dispersion curves (frequency versus wave vector) reveal critical information about bandgap locations, mode shapes, and the presence of localized or defect states, which are key to understanding wave manipulation in engineered media.

2.3.3. Key challenges in modeling internal interfaces

Accurate modeling of internal interfaces, such as those between inclusion and matrix materials or layered functional domains, is critical for predicting metamaterial performance. Key challenges include: (1) material discontinuities: sharp contrasts in density (ρ), stiffness tensor (c_{ijkl}), or piezoelectric coefficients can introduce discontinuities in the stress or displacement fields, complicating wave scattering and mode conversion; (2) continuity enforcement: for mechanical problems, continuity of displacement and traction must be satisfied; in piezoelectric systems, electric displacement (D) and electric field (E) must also be matched across interfaces; and (3) Bloch phase compatibility: in applying Bloch conditions, correct phase shifts are essential to ensure physical consistency. Inadequate implementation may result in spurious reflections or inaccurate dispersion predictions.

In conclusion, the combined application of FEA and Bloch's theorem offers a powerful and flexible framework for modeling periodic metamaterials. While FEA provides geometric and material adaptability, Bloch analysis enables the representation of infinite systems using finite domains. Together, they facilitate the design of structures with tailored bandgaps, enhanced attenuation, and engineered waveguiding properties, enabling innovations in vibration control, acoustic cloaking, energy harvesting, and biomedical systems. Looking forward, key research priorities include improving interfacial modeling accuracy, incorporating nonlinear and dynamic behaviors, and integrating machine learning and topology optimization for inverse metamaterial design. Such advances will accelerate the development of next-generation multifunctional metamaterials with unprecedented control over mechanical, acoustic, and electromagnetic wave phenomena.

3. Piezoelectric metamaterials: Technological advances and applications

Piezoelectric metamaterials, a novel class of smart materials that integrate the piezoelectric effect with engineered metamaterial architectures, have demonstrated significant potential across fields, including vibration control, energy harvesting, acoustic manipulation, and multifunctional structural design. In this section, we systematically review recent advances in piezoelectric metamaterials, with a focus on theoretical modeling, experimental validation, and numerical simulation. Key technological breakthroughs are highlighted in areas such as energy conversion, vibration mitigation, acoustic control,

and biomedical applications. Additionally, we analyze current challenges and outlines future research directions, offering valuable insights for researchers in related disciplines. For the readers' convenience, Table 1 lists representative bandgap characteristics of piezoelectric and phononic metamaterials.

Table 1. Representative bandgap characteristics of piezoelectric and phononic metamaterials.

Study/reference	Structure type	Frequency range (bandgap)	Bandgap width	Notable features
Chen et al. [34]	PMP-LR with local resonators	224–305 Hz	~80 Hz	Self-powered charge extraction improves energy harvesting
Sugino et al. [35]	Piezoelectric beam with synthetic impedance shunt circuits	1500–2200 Hz	~700 Hz	With synthetic impedance circuits
Xu et al. [36]	Piezoelectric plates with geometric cavities	3200–3280 Hz	~80 Hz	Broadened bandgap via cavity introduction
Wang et al. [2]	Acoustic metamaterial plate (flexural waves)	0–103 Hz	~100 Hz	Efficient flexural wave suppression
Gao et al. [37]	Plates with acoustic black holes + studs	1600–2300 Hz	~700 Hz	Black holes improve wave concentration
Pan et al. [38]	Shunted circuits with piezo transducers	505–510Hz	~5 Hz	Circuit optimization reduces uncertainty
Xu & Yan [39]	Dimension-dependent piezo-LC structure	Tunable (design-dependent)	~190 Hz	Dimension scaling impacts bandgap location

Notes: Bandgap width varies by resonator tuning, geometry, and circuit design. Studies often couple vibration suppression with energy harvesting, improving multifunctionality. The integration of nonlinear circuits or adaptive systems (e.g., RL control) shows promising adaptability for variable-frequency environments.

3.1. Theoretical modeling

In the realm of theoretical development, elastic-electromechanical coupling models have been extensively developed to investigate the bandgap characteristics of piezoelectric metamaterials and their influence on wave and vibration propagation. Strategies such as the integration of parallel inductors, capacitors, and tunable circuit components have significantly improved low-frequency broadband energy harvesting performance [34,40,41]. In particular, Chen et al. [34] explored a piezoelectric metamaterial plate with local resonators (PMP-LR, see Figure 5) to overcome the space limitations and high quality factor. Inspired by the hierarchical structure of natural bamboo, a new layered theoretical model has been proposed to enhance the effective Young's modulus of metamaterials [42]. Furthermore, through topology optimization and advanced geometric design, researchers have successfully tuned piezoelectric coefficients, overcoming the traditional limitation of only five non-zero coefficients in conventional piezoelectric ceramics [43]. Additional innovations, including the introduction of local resonators, geometric cavities, and segmented electrodes, have led to broader bandgaps and enhanced wave attenuation capabilities [36,44,45].

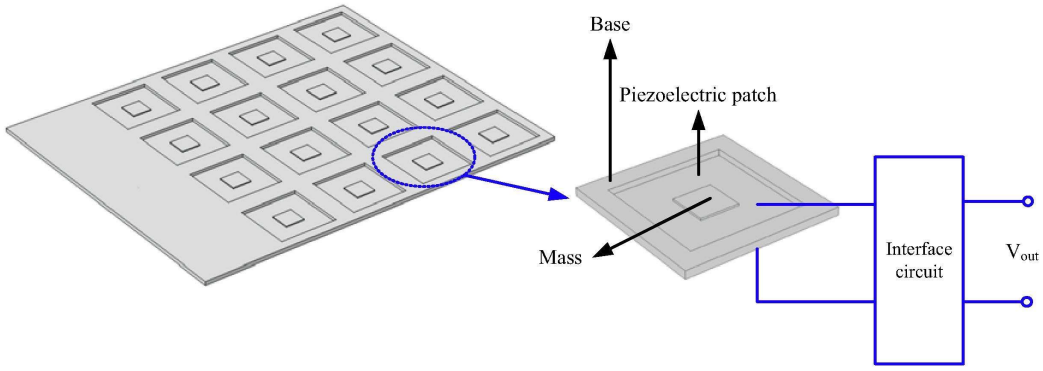

Figure 5. Basic configuration of a PMP-LR and its interface circuit (Reproduced from Ref. [34] with permission).

In the remainder of this section, we illustrate the theoretical modeling of piezoelectric metamaterials using a piezoelectric metamaterial plate with local resonators (PMP-LR) as an example, following the approach in [34]. As shown in Figure 5, the PMP-LR can be modeled as a two-dimensional Kirchhoff plate, thereby conforming to the classical Kirchhoff plate assumptions. All formulations presented here are adapted from [34].

Eq 17 represents Hamilton's principle, used to derive the dynamic equations governing the PMP-LR:

$$\delta \int_{t_1}^{t_2} (KE - PE)dt = 0 \tag{17}$$

where δ denotes the variational operator, *KE* is the total kinetic energy, and *PE* is the potential energy of the system.

The total kinetic energy *KE* in Eq 18 is composed of the contributions from the base structure (KE_s), the piezoelectric patches (KE_p), and the attached resonating masses (KE_m):

$$KE = KE_s + KE_p + KE_m = \frac{1}{2}\iint \left[\rho_s h_s + \left(\rho_p h_p - \rho_s h_s\right) S(x,y)\right] \left(\frac{\partial w}{\partial t}\right)^2 dxdy \tag{18}$$

where ρ_s and ρ_p are the mass densities, and h_s and h_p are the thicknesses of the base plate and the piezoelectric patches, respectively. The function *S(x,y)* is the indicator function that defines the spatial distribution of the *N* piezoelectric patches:

$$S(x,y) = \sum_{i=1}^{N} \left[H(x - x_{i,1}) - H(x - x_{i,2})\right] \left[\left[H(y - y_{i,1}) - H(y - y_{i,2})\right]\right] \tag{19}$$

In Eq 19, *H*(*) is the Heaviside unit step function, $(x_{i;1};\ y_{i;1})$ and $(x_{i;2};\ y_{i;2})$ are the coordinates of the bottom-left and top-right corners of the *i*-th cell unit, respectively.

Each piezoelectric patch operates in the 3–1 mode. Based on this, the electric displacement in the z-direction can be expressed as:

$$D_3(x,y,t) = e_{31}\varepsilon_1 + \bar{\varepsilon}_{33}^S E_3 \tag{20}$$

In Eq 20, $\bar{\varepsilon}_{33}^{S}$ is the permittivity at constant strain, D_3 is the electric displacement in the z-direction, E_3 is the electric field, e_{31} is the piezoelectric coefficient, and ε_1 is the mechanical strain in the corresponding direction.

Substituting Eq 19 into Eq 20, we obtain:

$$\frac{\partial D_3}{\partial z} = \frac{\partial}{\partial z}\left[\frac{h_s - h_p}{2} S(x,y) e^T (\Theta w) - S(x,y)\bar{\varepsilon}_{33}^{S}\frac{V}{h_p}\right] \tag{21}$$

In Eq 21, $\Theta = [\partial^2/\partial^2 x \quad \partial^2/\partial^2 y \quad 2\partial^2/\partial x \partial y]^T$.

The voltage V across the piezoelectric patch is determined by the electrical interface circuit. Unlike a pure resistive load, the interface circuit has a general impedance $Z(x)$, leading to

$$V(x,t) = Z(x)\frac{dQ(x,t)}{dt} \tag{22}$$

where Q is the electric charge generated by the piezoelectric effect.

Combining Eqs 21 and 22 with the governing equation provided in [34]:

$$m(x,y)\frac{\partial^2 w}{\partial t^2} + \Theta^T\left[C(\Theta w) + \frac{h_s - h_p}{4} S(x,y)\boldsymbol{e}V_p(t)\right] = F_0(x_0, y_0, t) \tag{23}$$

Using Eq 23, the coupled elastic-electro-mechanical model of the PMP-LR system (Eq 24) can be written as:

$$\begin{cases} m\frac{\partial^2 w}{\partial t^2} + \Theta^T\left[C(\Theta w) + \frac{h_s - h_p}{4} S(x,y) eV\right] = F_0 \\ \frac{\partial}{\partial z}\left[S(x,y)\left(\frac{h_s - h_p}{2} e^T(\Theta w) - \bar{\varepsilon}_{33}^{S}\frac{V}{h_p}\right)\right] \\ V(\omega) = j\omega Z(\omega) Q(\omega) \end{cases} \tag{24}$$

This model forms the theoretical foundation for analyzing the dynamic behavior of piezoelectric metamaterial plates with local resonators.

3.2. Experimental validation and application expansion

Leveraging advanced manufacturing techniques such as 3D printing and microcasting, piezoelectric metamaterials with complex geometries have been fabricated and experimentally validated in applications like energy harvesting, acoustic focusing, and vibration suppression. For instance, piezoelectric nanogenerators based on mechanical metamaterials utilize post-buckling deformation triggered by low-frequency excitation to achieve efficient energy conversion [7]. Tunable piezoelectric metamaterial prisms allow dynamic control of acoustic wave direction via inductive load adjustments, offering innovative solutions for beam steering [46,47].

3.3. Energy harvesting and conversion

In energy harvesting applications, researchers have significantly improved conversion efficiency through structural and circuit-level optimizations. For example, piezoelectric metamaterial plates equipped with self-powered synchronous charge extraction circuits and parallel inductors have

demonstrated up to a 200% increase in output voltage in low-frequency broadband environments [34]. Similarly, post-buckling mechanical metamaterial-piezoelectric nanogenerators (MM-PENG) effectively convert ambient mechanical energy into electricity (see Figure 6) [7]. Multi-axis energy harvesters based on embedded phononic crystal structures, encapsulated within a rubber matrix and reinforced with rigid frames, can extract energy from multi-directional, low-frequency vibrations with high efficiency [48].

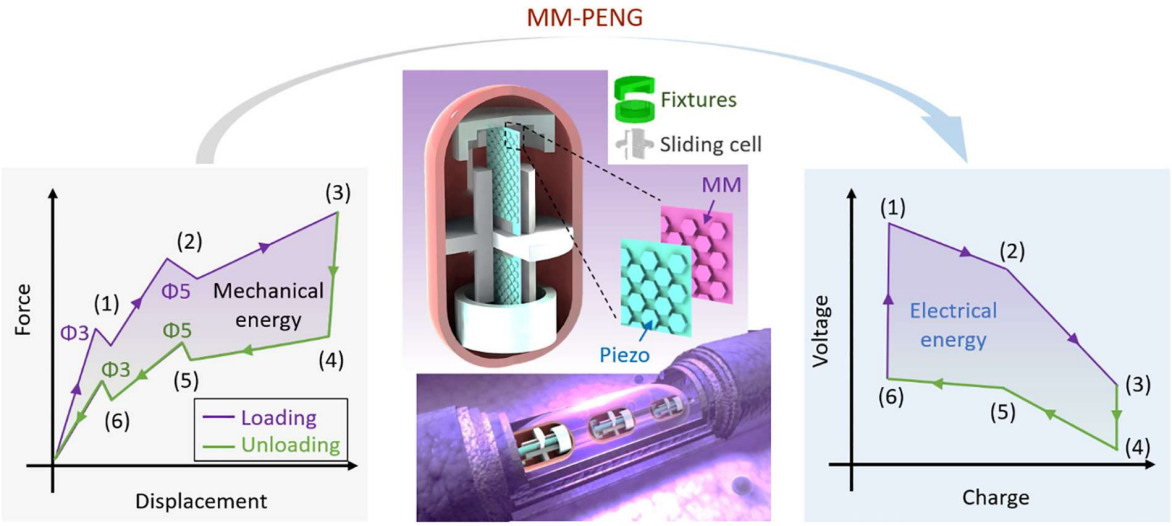

Figure 6. Schematics of the design principle and components of the MM-PENG, and the processes of energy harvesting and conversion through the post buckling response of the MM-PENG (Reproduced from Ref. [7] with permission).

3.4. Vibration control and suppression

Piezoelectric metamaterials exhibit significant potential for vibration suppression through bandgap engineering and damping mechanisms. By integrating local resonators or geometric cavities, metamaterial plates can be tuned to achieve low-frequency, broadband vibration attenuation [49]. Approaches such as nonlinear synchronized switch damping on inductors (SSDI) and multifunctional designs have been shown to generate wide phononic bandgaps for effective mitigation of low-frequency vibrations [50,51]. Bandgap width and performance have been further enhanced through size scaling, impedance matching, incorporation of piezoelectric transducers, and the use of multi-resonant piezoelectric shunting circuits [52–55], with additional bandgap designs explored in Refs. [56,57]. Notably, piezoelectric metamaterials can serve dual purposes—simultaneously harvesting energy and suppressing vibrations—by leveraging internal electromechanical coupling mechanisms that enhance both functionalities [58–61]. Recent studies have also demonstrated the energy harvesting capabilities of these systems under various operating conditions [62,63]. Moreover, reinforcement learning-based adaptive control strategies have been introduced to optimize performance in dynamically changing environments, further expanding their application potential [64].

3.5. Acoustic control and manipulation

In acoustic applications, piezoelectric metamaterials offer unique advantages in wave control and bandgap tuning. Tunable acoustic prisms, equipped with LC shunt circuits, enable dynamic steering of shear waves and targeted narrowband attenuation [46,65]. Technologies such as elastic wave frequency conversion and active control [66], as well as metamaterials embedded with piezoelectric rods [67], provide new approaches for ultrasonic noise suppression. Honeycomb-structured 3-3 piezoelectric metamaterials are utilized in hydrophone devices to reduce acoustic impedance [68]. Additionally, adaptive gradient-index (GRIN) lenses enable acoustic focusing via inductive load adjustment [69], while periodically perforated piezoelectric plate designs enable simultaneous vibration control and energy harvesting functionalities [70]. Beam steering is further refined through phase velocity control using piezoelectric LC circuits [47].

3.6. Biomedical applications

Piezoelectric metamaterials hold considerable promise in biomedical domains, particularly in biosensing, tissue engineering, and energy harvesting. Devices such as piezoelectric metamaterial infrared detectors, based on plasmonic nanostructures, offer high electromechanical responsiveness [63]. Applications span miniaturized and low power IR spectroscopy and multispectral imaging systems. [71], bioinspired flexible electrodes [72], and structural health monitoring (SHM) [73]. The potential for use in bone regeneration, pacemakers, and cochlear implants is also being actively explored [26,27]. Notably, bioinspired soft elastic metamaterials (BSEMs), modeled after the cochlea, enable natural hearing restoration through frequency separation and passive amplification of sound [16].

3.7. Broader applications and future prospects

Piezoelectric metamaterials have attracted growing interest in a wide range of emerging applications, including aerospace, automated SHM, and next-generation biomedical technologies. These materials offer unique advantages for targeted drug delivery, acoustic wave filtering, tissue engineering, and self-powered sensing systems [16,27,74]. Advances achieved optimizing flexoelectric-based metamaterials that mimic piezoelectricity through advanced modeling and genetic algorithms, alongside the development of a mechatronic metamaterial beam with LRC shunting circuits for tunable low-frequency vibration isolation, where both simulations and experiments confirm the critical role of electrical parameters in bandgap tuning [75,76]. Beyond piezoelectric systems, other categories of multi-field-responsive metamaterials are also gaining increasing attention. These include magneto-active metamaterials [77], thermo-responsive metamaterials [78], electro-active metamaterials [79,80], light-responsive elastic metamaterials [81], metasurfaces designed for high-performance photodetection [82]. These materials are paving the way for smart, adaptive, and reconfigurable systems with broad functionality.

A substantial body of foundational and specialized review literature offers deeper insights into the development and applications of piezoelectric metamaterials [26,27,73,74,83,84]. The methods discussed in this section exhibit distinct strengths and limitations. For clarity and ease of comparison, Table 2 summarizes the relative advantages and current challenges of each approach within this category.

Table 2. Comparative analysis of techniques in piezoelectric metamaterials.

Category	Design/technique	Advantages	Disadvantages
Energy harvesting mechanisms	Resonator-based designs (e.g., piezoelectric metamaterial plates with local resonators, PMP-LR)	•High energy conversion efficiency at specific frequencies •Suitable for structured environments with dominant frequency components	•Limited bandwidth •Requires precise tuning of resonator geometry and materials
	Broadband designs (e.g., MM-PENG)	•Wide operational frequency range •Effective for random or multi-directional vibrations	•Lower peak efficiency than resonator-based designs
Vibration suppression techniques	Bandgap control (e.g., piezoelectric plates with local resonators)	•Targeted attenuation of specific frequency bands •Ideal for isolating structures from harmful vibrations	•Narrow suppression bands •Sensitive to manufacturing tolerances
	Nonlinear damping (e.g., SSDI circuits)	• Broadband vibration mitigation via nonlinear effects •Adaptive to varying loads through synchronized switch damping	•Complex circuit integration •Potential energy dissipation as heat, lowering efficiency

4. Metamaterial-based biosensors: Technological advances and applications

In recent years, metamaterials, artificially engineered composites with tailored electromagnetic properties, have emerged as a powerful platform for biosensing applications. Their ability to precisely manipulate electromagnetic waves through subwavelength structural design enables substantial improvements in sensitivity, specificity, and detection limits. By fine-tuning their geometric configurations and optical/electromagnetic responses, researchers have developed a variety of high-performance, multifunctional metamaterial-based biosensors. These advanced sensors enable label-free, high-sensitivity detection of biomolecules and show promising potential in applications such as early cancer diagnosis, viral detection, food safety monitoring, and cellular state analysis. In this section, I review the latest developments in metamaterial-based biosensors across frequency domains, including THz, infrared (IR), visible light, and microwave, and highlights their technical innovations and application prospects in biomedical detection, protein analysis, and real-time cellular monitoring. It should be mentioned that metamaterial biosensors achieve high sensitivity through different resonance-enhancing mechanisms, each with distinct operating principles and advantages across frequency domains. Table 3 summarizes some sensitivity metrics of metamaterial-based biosensors.

Table 3. Sensitivity metrics of metamaterial-based biosensors.

Mechanism	Frequency or wavelength range	Typical sensitivity	Ref.
Plasmonic	40–45 GHz	130 nm/RIU	[85]
	2500–3500 nm	345 nm/RIU	[86]
	100–240 THz	560 nm/RIU	[87]
	350–800 nm	4800 nm/RIU	[88]
	700–3000 nm	1208 nm/RIU	[89]
	894–902 nm	360 nm/RIU	[90]
THz metamaterials	0–3 THz	370 GHz/RIU	[12]
	0.684–0.751 THz	67 GHz/RIU	[91]
	1000–2000 nm	173 nm/RIU	[92]
	0.2–1 THz	504 GHz/RIU	[93]
	1.1–1.5 THz	300 GHz/RIU	[94]
	0.4–1 THz	70 GHz/RIU	[95]
	1–1.8 THz	n/a	[96]

4.1. THz-frequency metamaterial biosensors

Metamaterial biosensors operating in the THz frequency range have proven particularly effective for detecting cancer biomarkers and viruses. Through optimized structural designs, such as double split-ring resonators (DSRRs), integrated with THz time-domain spectroscopy, researchers have developed sensors capable of detecting biomolecules like carcinoembryonic antigen (CEA) and alpha-fetoprotein (AFP) with detection limits as low as 0.25 ng/mL [93,97–100]. A novel water-based terahertz metamaterial biosensor integrated with a semiconductor film enables highly sensitive, label-free detection of skin cancer—achieving a refractive index sensitivity increase of 117 μm/RIU and a refractive index figure of merit over 20.53—through strong field localization and compatibility with biological tissues [101]. Graphene-based and phase-change-enabled H-shaped resonators allow dynamic modulation of absorption properties [102,103], enabling multi-band, high-sensitivity detection of glucose, proteins, malaria, dengue, early-stage disease biomarkers, and liver cancer-associated viral markers [104–107]. Additionally, THz metamaterial reflectors based on semiconductor thin films have been employed to detect avian influenza viruses—including H1N1, H5N2, and H9N2—with a sensitivity threshold as low as 1.67 pM [14]. For cellular analysis, THz metamaterial sensors—based on Fano resonance, aptamer-functionalized nanocomposites, or structures with luxuriant gaps—can detect normal epithelial cells (HaCaT) at concentrations as low as 0.2×10^5 cells/mL, demonstrating strong sensitivity in cell concentration detection [108–111].

4.2. Infrared-frequency metamaterial biosensors

In the infrared range, metamaterial sensors utilize mechanisms such as surface plasmon resonance (SPR) and Fano resonance to achieve ultra-sensitive, label-free detection. Plasmonic metamaterial absorbers fabricated via electron-beam lithography or designed with double plasmon-induced transparency (D-PIT) structures exhibit high absorption rates (up to 80%) and detection limits as low as 267.4 pM for proteins and other biomolecules [86,87]. These sensors are

also effective for deoxyribonucleic acid (DNA) detection, where metamaterial platforms incorporating SPR-based or asymmetric X-shaped resonator inclusions—optimized through precise gold layer thickness control and tailored structural configurations—exhibit significantly enhanced accuracy and signal responsiveness [92,112,113].

4.3. Visible-light metamaterial biosensors

Metamaterial sensors operating in the visible-light spectrum offer cost-effective, high-sensitivity solutions suitable for large-scale biomedical screening. Plasmonic metamaterials in this range have achieved sensitivities exceeding 4800 nm/RIU, significantly outperforming conventional sensors [88]. Asymmetric sword-shaped notched square resonator designs enable multi-band absorption with average absorption rates of 98.8%, providing novel approaches for multi-spectral detection and analysis [114].

4.4. Microwave-frequency metamaterial biosensors

Microwave-frequency biosensors have leveraged mechanisms such as trapped-mode resonance and plasmonic surface lattice resonance (PSLR) to detect organic and inorganic biological substances with high sensitivity. Complementary Ω-shaped resonator arrays can distinguish between healthy and cancerous tissues by analyzing dielectric and absorption differences [96]. PSLR-based microwave sensors further enhance sensitivity to refractive index changes, making them ideal for precise biomolecular detection [90].

4.5. Applications in food safety and toxin detection

Metamaterial-based sensors have also been applied in detecting food toxins and contaminants. Designs based on the Maxwell-Garnett effective medium theory and split-ring resonators enable high-sensitivity, label-free detection of aflatoxins B1 and B2 or streptavidin–agarose [115,116]. Additionally, THz-response-based fatty acid sensors exploit variations in molecular double-bond configurations to support advanced quality control in the food industry [117].

4.6. Viral detection and biomedical diagnostics

Metamaterial biosensors are increasingly being employed for the rapid detection of pathogens such as avian influenza, SARS-CoV-2, and hepatitis viruses. For example, THz sensors integrated with microfluidic chips and graphene coatings have demonstrated the ability to detect low concentrations of SARS-CoV-2 spike proteins and avian influenza viruses with high specificity and without the need for labeling [14,94,95,118]. These advances pave the way for rapid, real-time diagnostics in clinical and public health settings.

4.7. Cellular state monitoring

Studies have demonstrated the utility of metamaterial sensors in monitoring cellular hydration and viability. THz time-domain spectroscopy-based platforms can differentiate between normal and cancerous cells by analyzing intracellular hydration states and extracellular water dynamics. These

systems facilitate real-time monitoring of cell viability, biomolecule interactions, and bovine serum albumin detection in small-volume liquid samples, while also responding to external stimuli—providing powerful tools for biomedical research and diagnostic applications [119–122]. For further insights into metamaterial-based biosensors and their applications, comprehensive reviews are available in [123–126], and Microfluidic as well as optical biosensors in particular [123,127].

4.8. Key physical mechanisms underlying high sensitivity in metamaterial biosensors

The remarkable sensitivity of metamaterial-based biosensors, particularly in the THz and IR regimes, stems from their capacity to manipulate electromagnetic waves at subwavelength scales using precisely engineered micro- and nanostructures. This section reviews three fundamental physical mechanisms that underpin their performance in biomolecular detection: localized surface plasmon resonances (LSPR), spoof surface plasmons, and dielectric resonator modes.

4.8.1. LSPR

LSPR occurs when incident light excites collective oscillations of conduction electrons in metallic nanostructures (e.g., gold or silver), resulting in the formation of highly confined electromagnetic fields, commonly referred to as "hot spots". These regions exhibit extraordinary sensitivity to perturbations in the surrounding dielectric environment, such as those caused by biomolecular binding, making LSPR an exceptionally effective mechanism for biosensing. In the THz regime, LSPR is typically engineered using subwavelength structures such as SRRs, asymmetric H-shaped units, or similar metamaterial elements. Upon biomolecule adsorption, changes in the local refractive index induce measurable shifts in the resonant frequency, enabling label-free detection of biomarkers [12,93]. In the IR regime, plasmonic metamaterial absorbers—such as gold nanorod arrays—achieve enhanced absorption efficiency and ultrasensitive detection by leveraging nanogap-induced electromagnetic field enhancement [82–85]. More advanced platforms, such as graphene-integrated THz metamaterials, utilize electrostatic gating to dynamically tune plasmonic resonances, enabling attomolar-level detection of cancer biomarkers and achieving up to 80% absorption at infrared wavelengths [85,86,91,128].

4.8.2. Spoof surface plasmons

Spoof surface plasmons are artificially engineered, surface-bound electromagnetic modes designed to emulate the behavior of optical surface plasmons at lower frequencies, such as in the THz and microwave regimes. These modes are typically supported by periodically structured metallic surfaces, such as grooved or perforated arrays, and are characterized by strong electromagnetic field confinement and extended propagation lengths.

A key application of spoof surface plasmons lies in biosensing. In particular, spoof plasmonic waveguides integrated with microfluidic systems have enabled label-free detection of viruses by monitoring resonance frequency shifts upon pathogen binding. For instance, this approach has successfully detected the H1N1 virus at low concentrations [14,94]. By circumventing the diffraction limit, these platforms support high-density integration, facilitating the development of compact and multiplexed biosensor arrays. A notable example is a highly sensitive terahertz biosensor for avian influenza virus detection, based on spoof surface plasmon polaritons supported by a grating-coupled

metamaterial structure with slow-wave transmission lines, achieving strong field confinement, a high Q-factor of 690 at 1.93 THz, and up to 8% average sensitivity through optimized geometries and full-wave simulation validation [94]. These advancements underscore the potential of spoof surface plasmons as a foundation for highly sensitive, miniaturized biosensing technologies.

4.8.3. Dielectric resonator modes for biosensing

Dielectric resonators, typically composed of high-refractive-index materials such as silicon or titanium dioxide (TiO_2), support low-loss electromagnetic resonances, most notably Mie-type electric and magnetic dipole modes. Unlike their metallic counterparts, dielectric structures significantly reduce ohmic losses while offering inherent biocompatibility, making them highly suitable for biosensing applications. In both the infrared and visible regimes, all-dielectric metasurfaces leveraging Mie resonances have demonstrated exceptional performance in label-free detection, with reported sensitivities up to 4800 nm/RIU for applications including bioimaging, gas sensing, and contamination monitoring—highlighting their potential for ultrasensitive molecular diagnostics. Additionally, a five-band metamaterial absorber based on a metal–insulator–metal array of gold nano-crosses achieves absorption from 700–3000 nm with over 99% peak efficiency, polarization and angle insensitivity, and strong suitability for label-free biosensing [88,89]. In the THz regime, incorporating dielectric layers has been shown to enhance the resonator quality (Q) factor, thereby improving detection resolution, particularly in applications such as real liquid-based biosensing [121,129]. A prominent example includes a fast, simple, and label-free terahertz metamaterial biosensor with luxuriant gaps enabling high-sensitivity detection and distinction of various cells and bacteria—including glioblastoma, Candida albicans, Escherichia coli, and Shigella dysenteriae—demonstrates strong potential for early diagnosis and advanced cell biology research [110]. These developments underscore the promise of dielectric resonators as a low-loss, high-sensitivity platform for next-generation biosensing technologies.

Table 4. Comparative advantages and challenges.

Feature	LSPR	Spoof plasmons (SSPs)	Dielectric modes (Mie resonances)
Frequency range	Visible–NIR	THz–microwave	Visible–NIR–Mid-IR
Losses	High (Ohmic)	Low (PEC-like)	Very low (dielectric)
Field enhancement	Strong	Moderate	Modest
Electric/magnetic response	Primarily electric	Electric-like	Both electric and magnetic
Fabrication complexity	High (nano)	Moderate (micro)	Moderate–high (nano)
Integration with electronics	Moderate	High (RF/PCB compatible)	High (CMOS-compatible)
Tunability	Broad via shape/material	Broad via structural design	Limited (size/shape tuning)
Application strengths	Sensing, nonlinearity	THz optics, bioimaging, antennas	On-chip photonics, biosensing, metasurfaces

By leveraging these physical mechanisms, metamaterial biosensors have achieved remarkable performance in ultrasensitive, label-free, and real-time biomolecular detection. Table 4 summarizes the key advantages and challenges associated with each sensing mechanism. Their integration with microfluidics, flexible substrates, and on-chip electronics further enables the development of wearable, implantable, and point-of-care diagnostic platforms, advancing personalized medicine, pandemic response, and environmental monitoring. To aid comparative understanding, Tables 5 and 6 provide a comprehensive overview of the strengths and limitations of various metamaterial-based biosensing approaches, highlighting their practical benefits and technical challenges.

Table 5. Comparison of sensor architectures in metamaterial biosensors.

Feature	Planar resonators (e.g., SRRs)	3D resonators (e.g., chiral/helical)	Photonic crystal cavities (PhC cavities)
Sensitivity	High	Very high	Very high (particularly near-surface)
Selectivity	Moderate to high	High (especially for chiral analytes)	Moderate
Q-factor/resolution	Moderate	High	Ultra-high
Spectral tunability	Moderate	High	Moderate
Fabrication complexity	Low to moderate	High (multi-layer alignment, 3D lithography)	Very high (nanometer precision required)
Integration compatibility	Excellent (CMOS-compatible, scalable)	Moderate to low	Excellent (on-chip integration possible)
Miniaturization	Good	Challenging	Excellent (sub-wavelength footprints)
Sensing volume	Moderate (surface and near-field)	Moderate to high (volume + chiral interaction)	Low (extreme confinement near cavity surface)
Detection depth	Surface and near-surface	Surface + partial volume	Surface-dominant (within evanescent field)
Target analytes	General biomolecules, pathogens	Chiral molecules, asymmetric binding targets	Small molecules, protein markers, label-free cell sensing
Application examples	Protein markers, pathogens, BSA detection	Glucose isomers, DNA chirality, virus enantiomers	Glioblastoma cells, Candida, E. coli, Shigella detection

Table 6. Comparison of frequency-domain metamaterial biosensors: microwave vs. THz vs. IR sensors.

Feature	Microwave sensors	THz sensors	IR sensors
Water compatibility	✅ Excellent (low attenuation)	❌ Poor (strong water absorption)	⚠️ Moderate (some interference in mid-IR)
Tissue penetration depth	✅ High	❌ Shallow	⚠️ Low
Molecular specificity	⚠️ Low (requires surface functionalization)	✅ Moderate (fingerprinting possible)	✅ High (vibrational fingerprinting)
Spatial resolution	❌ Low (long wavelengths)	⚠️ Moderate	✅ High (sub-micron possible with metasurfaces)
Label-free capability	⚠️ Limited (dependent on indirect detection)	✅ Yes	✅ Yes
In-liquid detection capability	✅ Excellent	❌ Poor	⚠️ Moderate (limited in aqueous media)
Instrumentation cost	✅ Low to moderate	❌ High	⚠️ Moderate to High
Integration potential	✅ Excellent (with flexible substrates, microfluidics)	⚠️ Moderate (lab setups dominate)	✅ Good (chip-scale platforms possible)
Real-time sensing	✅ Yes	✅ Yes	✅ Yes
Environmental sensitivity	⚠️ Susceptible to EMI and temperature drift	✅ Low	⚠️ Thermal noise considerations
Suitability for wearables	✅ Strong	❌ Weak	⚠️ Limited
Representative applications	Hydration sensors, dielectric spectroscopy, food quality	Virus detection, glucose, bacteria	Protein analysis, cancer markers, chemical ID

Note: ✅ = Strong advantage; ⚠️ = Moderate/conditional; ❌ = Limitation.

5. Bioinspired metamaterials: Technological advances and applications

Bioinspired metamaterials represent a novel class of smart materials that synergistically integrate principles from biomimetics and metamaterial science. These materials draw inspiration from nature's intricate structures and multifunctional capabilities, offering promising solutions across fields such as materials science, engineering, and biomedical technology. By mimicking biological architectures, researchers have engineered metamaterials with enhanced mechanical, optical, and adaptive functionalities. In this section, I review recent progress in bioinspired metamaterials, with a focus on their applications in antifouling, mechanical modulation, optical enhancement, and beyond.

5.1. Antifouling technology

Inspired by the microstructures of snail shells, researchers have fabricated nanopillar arrays on silicon wafers and resin films that exhibit excellent oil-repellent and antifouling behavior in aqueous environments. These surfaces have been successfully applied to bile duct catheters, demonstrating significant antifouling performance in porcine models [130,131]. This advancement provides

valuable insights into improving the longevity and biocompatibility of medical implants by reducing biofilm formation.

5.2. Mechanical property modulation

Bioinspired mechanical metamaterials, often realized through 3D printing, leverage nature-inspired geometries to enhance structural performance. For instance, interlocking structures based on Koch fractal geometry have demonstrated superior load-bearing capabilities in both experimental and simulation settings [132]. Chiral mechanical metamaterials with sequential unit-cell activation under large strain have shown potential in applications like drug delivery systems [133,134]. Modular origami and kirigami-based designs enable the decoupling of global structure from local mechanical function, enabling independent control of each voxel's properties in 1D, 2D, and 3D configurations [135]. Wang et al. [136] introduced an overdamped metamaterial system that exploits rotational buckling in curved beam units to confine impact energy and enhance energy dissipation. Additionally, Zeng et al. [137] proposed a deep learning-based inverse design strategy for gradient mechanical metamaterials, enabling rapid customization of microstructures with prediction accuracies reaching 99.09%.

5.3. Optical performance enhancement

Bioinspired photonic metamaterials have shown remarkable potential in enhancing nonlinear optical responses. By emulating the microstructure of animal bones, researchers have overcome the traditional trade-off between resonance speed and efficiency [138]. Chen et al. [139] reviewed the development of soft optical metamaterials using flexible materials such as liquid crystals, fluids, and polymers, highlighting their tunability and adaptability. Drawing inspiration from butterfly wings and moth-eye patterns, Duan et al. [140] designed a dual-structured system comprising porous and convex arrays, and fabricated carbonyl iron–polyurethane metamaterials (CSMA) with effective wave-absorbing capabilities (see Figure 7). These structures offer new approaches for optical stealth, filtering, and broadband light manipulation.

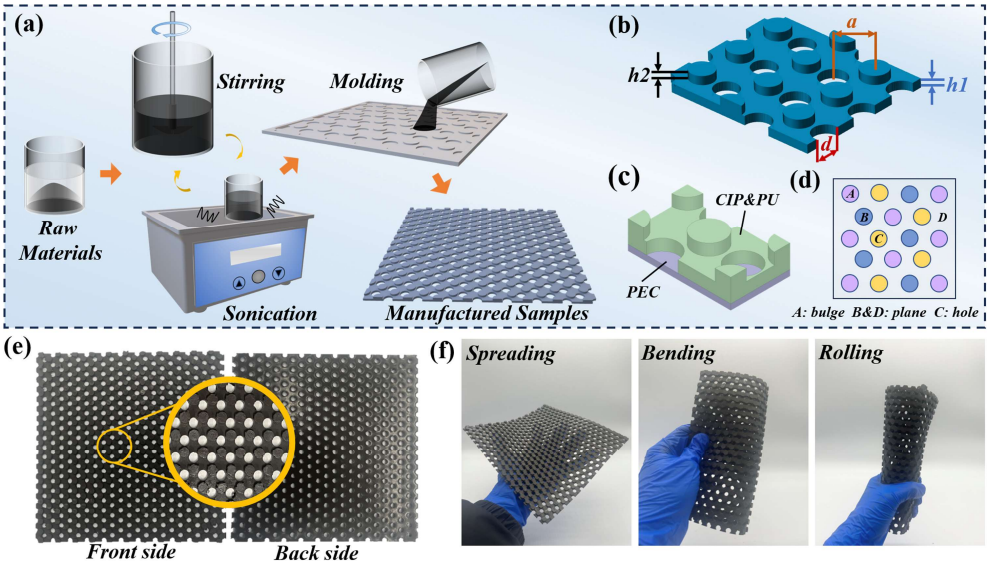

Figure 7. (a) Schematic of the preparation process. (b) Schematic of the dimensional parameters of CSMA. (c) Periodic repetition unit used for software simulation. (d) Schematic of 2D planar distribution of CSMA structural elements. (e, f) Physical photographs of CSMA (Reproduced from Ref. [140] with permission).

5.4. Shape memory and transformable metamaterials

Advanced shape-changing metamaterials have been realized using 4D printing techniques. For instance, Li et al. [141] developed dome-array structures capable of dynamic deformation, while Silva et al. [142] embedded ferromagnetic nanoparticles in elastic films arranged in rotating square origami geometries, creating intelligent, magnetically responsive soft metamaterials.

5.5. Advanced manufacturing techniques

The advent of multi-material 3D printing has greatly facilitated the fabrication of complex bioinspired structures. Triangular suture-inspired patterns, for example, reveal the influence of tooth angles and interfacial material strength on failure modes under uniaxial loading, thereby enhancing mechanical integrity [132–134,143]. Origami and kirigami-inspired designs enable voxel-level customization, decoupling global morphology from local function [135]. Wang et al. [72] introduced a novel "Boolean Logic-guided Microcasting-based 3D Stereolithography" technique, enabling the assembly of more than 20 types of challenging multi-material metamaterials with high precision and efficiency.

5.6. Multifunctional integration and intelligent control

Bioinspired metamaterials increasingly incorporate smart responsiveness and multifunctionality. For instance, field-responsive mechanical metamaterials filled with magnetorheological fluids enable remote modulation of stiffness via external magnetic fields, opening new avenues for smart and adaptive systems [144]. In parallel, deep reinforcement learning has been applied to optimize

moth-eye-inspired structures for ultra-broadband perfect absorption, significantly improving the efficiency and effectiveness of design processes [145].

5.7. Bioinspired structural design and fabrication

Nature remains a central guide in the design of advanced metamaterials. Numerous studies [146–149] have replicated structural features of organisms such as snail shells using advanced design and precision fabrication techniques like 3D printing and laser melting. Jiao et al. [21], for example, developed an origami-metamaterial hybrid bouquet that mimics flower blooming through programmable structural transformations. Wang et al. [150] introduced a Kagome-Gyroid hybrid structure that combines the high shear resistance of Kagome lattices with the excellent strength-to-weight ratio of Gyroid lattices, offering a promising platform for lightweight, high-performance structural materials.

5.8. Structural motifs in bioinspired metamaterials: Mechanisms and mechanical enhancements

The exceptional mechanical performance of bioinspired metamaterials arises from the incorporation of structural motifs such as chirality, hierarchical organization, and auxetic geometry. These design principles, drawn from nature, not only mimic biological systems but often exceed the mechanical limitations of conventional materials. They enable tailored responses to mechanical stimuli, offering multifunctionality that is particularly advantageous in biomedical applications. In this section, I highlight the underlying mechanisms and functional benefits of each motif, supported by theoretical and experimental studies.

5.8.1. Chirality: Twist-dominated deformation

Chiral structures are characterized by geometric asymmetry, typically manifesting as left- or right-handedness, that induces a coupling between axial loading and rotational deformation. This twist-dominated mechanical response enables energy dissipation primarily through shear and torsion, rather than direct axial strain, offering distinct performance advantages. For example, chiral unit cells with helical or spiral geometries dissipate mechanical energy efficiently via rotational buckling. Jiang et al. [133] demonstrated sequential cell-opening mechanisms over a wide range of overall strain, from 2.91% to 52.6%.

In addition, the strain-dependent sequential activation of chiral elements allows for tunable stiffness gradients, making these structures well-suited for applications such as soft robotics and controlled drug delivery systems [134]. Chiral architectures also inherently support a negative Poisson's ratio, enabling lateral expansion under axial tension, a behavior that mimics the mechanics of biological soft tissues like tendons and skin, thereby enhancing biomechanical compatibility. A notable example is the metamaterial featuring chiral cells and re-entrant cores [133], which exhibits a Poisson's ratio of −0.65. This characteristic makes it especially suitable for load-bearing biomedical implants that demand both fracture resistance and adaptive compliance.

5.8.2. Hierarchical design: Multi-scale toughening

Hierarchical architectures emulate natural materials such as nacre and bone by incorporating structural features across multiple length scales, from nano to macro, thereby enhancing toughness, energy dissipation, and mechanical efficiency, even when composed of intrinsically brittle constituents. One key advantage is crack deflection and arrest, facilitated by multi-scale interfaces that interrupt crack propagation. For example, beetle-inspired suture-like microstructures [18] have inspired new approaches for the development of advanced bioinspired applications. Liu et al. [143] reported that 3D-printed triangular suture specimens revealed a transition from tooth breakage to interfacial cohesive failure depending on geometry and material properties, as confirmed by experiments and nonlinear finite element simulations. Inspired by the macro–micro deformation behavior of natural biomaterials, a novel class of hierarchical auxetic-hexagonal (AuxHex) metamaterials with substructures such as equilateral triangles and double arrowhead cells was developed [8], leading to enhanced load-bearing capacity and energy absorption. A universal plastic collapse stress model, free from redundant fitting parameters, was proposed to predict the mechanical performance across various hierarchical designs, and validated by experiments and simulations on laser-melted stainless steel specimens. Moreover, synergistic toughening is achieved by combining stiff (e.g., ceramic) and compliant (e.g., polymer) phases at multiple scales, resulting in enhanced toughness without significant loss of strength. This is exemplified in pomelo peel–inspired structures [20], which replicate hierarchical cellular arrangements for impact resistance. A notable example is the Kagome–Gyroid (K–G) hybrid lattice [150], which introduces a novel interpenetrating K–G structure that merges the shear resistance of the Kagome lattice with the high specific strength and stiffness of the Gyroid lattice, drawing inspiration from naturally strong yet lightweight biomimetic structures such as butterfly wings and cancellous bone. Demonstrating up to 49.5% greater specific energy absorption and 35.6% improved energy absorption efficiency, the K–G structure offers significant advantages for high-impact applications in aerospace, rail transportation, and automotive industries.

5.8.3. Auxetic geometry: Enhanced energy dissipation

Auxetic structures, such as re-entrant honeycombs and double-arrowhead lattices, are characterized by a negative Poisson's ratio, which results in lateral expansion under tensile loading and densification under compression. This counterintuitive deformation behavior significantly enhances mechanical resilience and energy absorption, offering distinct advantages for biomedical applications.

First, under compressive loads, auxetic architectures exhibit uniform densification, allowing efficient dissipation of impact energy through controlled pore collapse. For instance, Wang et al. [136] demonstrated that overdamped auxetic lattices can achieve an impact displacement attenuation rate of up to 91.5%. Second, meta-biomaterials—an emerging subset of metamaterials with distinctive mechanical, mass transport, and biological properties—have shown significant potential in biomedical applications [10], particularly in orthopedic tissue repair and replacement, where fatigue resistance under cyclic musculoskeletal loading is crucial. This paper reviews recent progress in understanding the fatigue behavior of metallic meta-biomaterials, covering analysis techniques, key influencing factors such as topology and material composition, and predictive models for crack propagation and fatigue life, with the goal of informing future research and supporting clinical translation.

In addition, auxetic materials offer enhanced fracture resistance by expanding laterally around crack tips, which redistributes stress and delays crack propagation. For example, Shirzad et al. [4] developed a gradient triangular auxetic structure that exhibited a 13% increase in compressive Young's modulus and a 35% increase in compressive yield strength compared to a conventional triangular auxetic structure.

By leveraging these structural motifs, bioinspired metamaterials offer transformative potential for a wide range of biomedical applications, from smart implants to adaptive prosthetics. To enable successful clinical translation, future research should prioritize standardized mechanical testing protocols, thorough biocompatibility assessments, and comprehensive in vivo validation. Table 7 provides a summary of the key structural features, underlying mechanisms, and associated biomedical applications.

Table 7. Comparative summary of structural motifs in biomedical applications.

Structural motif	Key structural features	Underlying mechanisms	Biomedical applications
Chirality	-Asymmetric geometry -Helical or twisted micro/nanostructures (e.g., collagen, DNA) -Left-/right-handed configurations	-Induces optical activity -Influences mechanical behavior (torque, twist) -Enables cell–substrate mechanical feedback through asymmetric force distributions	-Chiral scaffolds enhance cell alignment, differentiation, and tissue regeneration -Chiral nanoparticles used in targeted drug delivery and biosensing due to enantioselective interactions
Hierarchy	-Multi-scale organization (nano→micro→macro) -Repeating motifs across length scales (e.g., bone, nacre) -Often combines multiple structural motifs	-Enhances mechanical robustness via synergistic deformation modes -Offers gradients in stiffness, porosity, and composition -Facilitates mechanotransduction	-Bone and cartilage scaffolds mimicking hierarchical organization for load-bearing implants -Tissue engineering matrices with gradient cues for cell migration and angiogenesis
Auxeticity	-Negative Poisson's ratio structures (e.g., re-entrant honeycombs, rotating units) -Expand laterally when stretched	-Strain-induced lateral expansion redistributes stress -Local rotation or hinging units accommodate deformation -Improves energy absorption and fracture resistance	-Stents, wound dressings, and prosthetics with improved conformability and mechanical cushioning -Auxetic scaffolds promote uniform cell distribution and mechanical stimulation during tissue growth

5.9. Structural stability vs. functional instability: Harnessing mechanical instabilities in metamaterials

The interplay between structural stability and functional instability is a hallmark of next-generation metamaterial design. While mechanical instabilities, such as buckling, snap-through, and bi-stability, are typically viewed as failure modes in conventional materials, they can be deliberately engineered in metamaterials to enable novel, adaptive functionalities [151–153]. In this subsection, we explore how

such instabilities are either mitigated to ensure reliability or purposefully exploited for transformative biomedical and adaptive applications.

5.9.1. Instabilities as performance limiters

Auxetic lattices, such as re-entrant honeycombs, are prone to premature buckling under compressive loads due to their slender struts and high porosity, which undermines their energy absorption capacity and resistance [154]. Similarly, shape-memory metamaterials—such as 4D-printed domes and asymmetric split-ring resonator architectures—can exhibit uncontrolled snap-through instabilities during rapid phase transitions, which may compromise actuation precision and reliability in applications like drug delivery and soft robotics [141,155]. In contrast, field-enhancement metamaterials incorporating a graphene-coated, reconfigurable SRR nano-aperture antenna—modeled using the finite-difference time-domain method in CST (Computer Simulation Technology) Microwave Studio—demonstrate enhanced transmittance and directional sensitivity for biomedical and spectroscopic applications, with performance tuned via SiO_2 nanosphere arrays and substrate/nanomaterial configurations [156].

To address these challenges, researchers have turned to topology optimization techniques, often enhanced by deep learning algorithms [137], to refine unit cell geometries by tuning parameters such as strut thickness, curvature, and connectivity. Material hybridization strategies, such as integrating stiff Ti-6Al-4V or CoCrMo alloys with compliant elastomers in functionally graded configurations, have been shown to improve buckling resistance or facilitates personalised stiffness-matching while maintaining desirable auxetic responses [157,158]. Furthermore, the use of overdamped metamaterial designs [136], which incorporate energy-dissipating mechanisms like rotational buckling, can effectively suppress catastrophic failure under dynamic loading conditions.

5.9.2. Instabilities as functional enablers

Mechanical instabilities, traditionally viewed as failure modes, are increasingly being harnessed in metamaterials to enable transformative functionalities. Controlled buckling in chiral and hierarchical architectures, such as K–G hybrids [150], facilitates localized stress redistribution, enabling a 49.5% increase in specific energy absorption and a 35.6% improvement in energy absorption efficiency compared to conventional materials, highlighting its superior potential for high-impact applications. Auxetic meta-biomaterials [159], engineered to exhibit a negative Poisson's ratio, offer a promising solution for durable bone implants. Their tunable mechanical and morphological properties, combined with exceptional fatigue resistance, have been demonstrated in additively manufactured titanium structures with varying geometries and relative densities. Meanwhile, cancer-affected brain tissues can be identified by their unique metamaterial properties, such as effective permittivity. This approach introduces a novel diagnostic paradigm by modeling biological tissues as disordered metamaterials, potentially enabling earlier and more accurate tumor detection than conventional pathological methods [160]. Bistable origami and kirigami structures [21] combine biomimicry with information processing over time for floriography inthe spatiotemporal 4D. Naify et al. [161] introduced a compact, geometrically simple metamaterial-based acoustic vortex generator capable of producing multiple orthogonal orbital angular momentum modes using a single transducer, offering a tunable and integrable alternative to traditional systems for applications in high-bit-rate acoustic communications and biomedical devices like microfluidic mixers. Likewise,

auxetic scaffolds that exhibit buckling-induced pore closure can modulate mechanical stiffness throughout the bone healing process, offering stage-specific mechanical support [162,163]. By reframing mechanical instability as a design opportunity than a limitation, metamaterials can be engineered to deliver novel functionalities in biomedical contexts, from energy-dissipating orthopedic devices to self-actuating surgical tools. Future efforts must address key challenges such as long-term cyclic durability, fatigue resistance, and seamless in vivo integration to enable successful clinical translation. Table 8 provides design paradigms for balancing stability and functionality.

Table 8. Instability-informed design paradigms for biomedical metamaterials.

Instability type	Strategic function	Associated risks	Design principles
Buckling	-Energy absorption (e.g., impact-mitigating orthopedic implants) -Controlled deformation for adaptable prosthetics -Soft robotic actuators	-Unintended or premature failure -Geometric sensitivity to imperfections -Post-buckling instability leading to loss of control	-Use post-buckling control via material gradients or boundary constraints -Incorporate geometric tuning (e.g., beam slenderness, curvature) -Employ finite element modeling for nonlinear stability prediction
Snap-through	-Rapid deployment or release (e.g., stent deployment) -Switchable drug delivery systems -Self-actuating surgical tools	-High stress concentrations at transition points -Difficult to reverse without active control -Fatigue under cyclic loading	-Optimize snap-through threshold via hinge geometry or prestress -Integrate soft–stiff material interfaces to reduce stress -Control with stimuli-responsive elements (thermal, pH, magnetic)
Bistability	-Stable configuration switching (e.g., implant shape memory) -Long-term retention without constant energy input	-Limited reversibility if hysteresis is large -Unpredictable transitions under external perturbations -Difficult to tune intermediate state	-Engineer energy landscapes with double-well potentials -Use multimaterial architectures to control transition barriers -Design for reversible actuation cycles with safety margins

5.10. Nacre-like metamaterials for elastic wave control and bandgap engineering

Nacre-inspired metamaterials, modeled after the hierarchical brick-and-mortar microarchitecture of natural nacre, have emerged as promising platforms for elastic wave manipulation due to their unique structural anisotropy, periodicity, and energy-dissipating interfaces. These metamaterials typically consist of hard platelets (e.g., ceramics or stiff polymers) embedded in a soft, viscoelastic matrix, mimicking the natural arrangement of aragonite tablets within biopolymeric layers. The contrast in mechanical impedance between the two phases creates periodic discontinuities, enabling effective bandgap formation and wave attenuation over target frequency ranges. Design strategies often involve tuning the aspect ratio, spacing, and interfacial compliance between platelets to modulate wave propagation behavior. For instance, De Maio et al. [164] revealed that finite deformation effects in bioinspired periodic composites induce multiscale nonlinear behaviors and instabilities, enabling

the design of highly deformable metamaterials with tunable elastic wave attenuation through strategic microstructural features like voids and lead inclusions.

Applications of nacre-like metamaterials extend fields. In structural health monitoring, their ability to filter or redirect elastic waves makes them useful in suppressing unwanted vibrations or enhancing signal clarity in sensors. In biomedical implants, they offer mechanical compatibility and wave-damping capabilities, minimizing mechanical noise in diagnostic imaging or wearable devices. Nacre-like designs have also been explored in phononic crystal engineering, where deliberate architectural modifications, such as hierarchical layering, chirality, or porosity, enable sophisticated waveguiding, mode conversion, and frequency-selective filtering. Advanced fabrication methods, such as multi-material 3D printing and layer-by-layer assembly, have facilitated the realization of nacre-like designs with spatially graded bandgap properties and direction-dependent attenuation.

Table 9. Comparative analysis of techniques in bioinspired metamaterials.

Category	Design/technique	Advantages	Disadvantages
Mechanical design strategies	Auxetic structures (e.g., negative Poisson's ratio materials)	•Enhanced energy absorption and fracture resistance •Mimics bone mechanics for implants •Adaptive deformation reduces stress shielding in orthopedic applications	•Limited biocompatibility of metallic auxetics (e.g., Ti-6Al-4V) due to corrosion •Complex 3D printing needed for intricate geometries
	Chiral/origami designs	•Programmable shape transformation (e.g., 4D-printed dome arrays) •Suitable for dynamic biomedical devices (e.g., drug delivery) •Modular designs enable voxel-level control	•Structural instability under cyclic loading •Limited load-bearing capacity vs. traditional materials
Fabrication techniques	3D printing (e.g., fused deposition modeling, stereolithography)	•High design flexibility for complex bioinspired geometries (e.g., Koch fractals) •Rapid prototyping for customized implants	•Layer-by-layer process may introduce defects •Limited biocompatible material options (e.g., polylactic acid vs. medical-grade polymers)
	Microcasting/nanofabrication	•Precise control over nanoscale features (e.g., moth-eye anti-fouling surfaces) •High reproducibility for mass production	•Scalability issues for large structures •Expensive equipment requirements

Studies (e.g., [164–166]) have further shown that exploiting micro-instabilities and wave filtering within nacre-like architectures under compressive loading can lead to reconfigurable bandgap behavior, effectively turning mechanical instabilities into functional design elements. Such concepts pave the way for smart nacre-like metamaterials capable of adaptive wave control in response to environmental stimuli, with potential applications in aerospace, civil infrastructure, and acoustic stealth technologies.

Each approach discussed in this section presents unique strengths and limitations. For the reader's convenience, Table 9 offers a concise comparison, summarizing the key advantages and current challenges associated with each method within this category.

6. Biometamaterials: Technological advances and applications

Biometamaterials are an emerging class of engineered materials specifically designed to interact with biological systems through tailored structural, mechanical, electromagnetic, and biochemical properties. Enabled by advanced fabrication methods such as additive manufacturing and nanoscale patterning, these materials enable unprecedented control over biological interactions. This section presents recent technological breakthroughs and highlights the expanding applications of biometamaterials in biomedical science and engineering.

6.1. Biomedical detection

Biometamaterials have shown remarkable promise in biomedical detection due to their unique electromagnetic and optical properties, enabling highly sensitive and selective diagnostic platforms. For instance, THz biosensors based on Fano resonance can detect cell concentrations as low as 0.2×10^5 cells/mL by monitoring shifts in resonance frequency [108]. THz metamaterial sensors also exhibit high sensitivity and specificity in detecting skin cancer and bovine serum albumin as well as in achieving near-unity absorbance over a wide range of incident angles [15,156,167], facilitating rapid, label-free, and portable diagnostics and power absorbers. Furthermore, glioma detection using metamaterials is achieved by analyzing variations in the effective dielectric properties of tissues, enabling accurate discrimination between healthy and malignant regions [160].

6.2. Optical and electromagnetic devices

The multifunctional and tunable characteristics of biometamaterials have broadened their application in optical and electromagnetic systems, including imaging, spectroscopy, and wave manipulation. Polarization converters and photodetectors based on metamaterials provide broadband, efficient polarization conversion [168–170], while graphene-integrated absorbers dynamically adjust absorption peaks through Fermi level modulation [171]. Additionally, metamaterial-based acoustic vortex beam generators produce orthogonal orbital angular momentum modes for microfluidic biomedical applications, such as mixing and sorting [161]. All-dielectric metamaterials (see Figure 8) exhibiting electromagnetically induced transparency have also demonstrated high sensitivity and figure-of-merit in THz sensing applications [155,172].

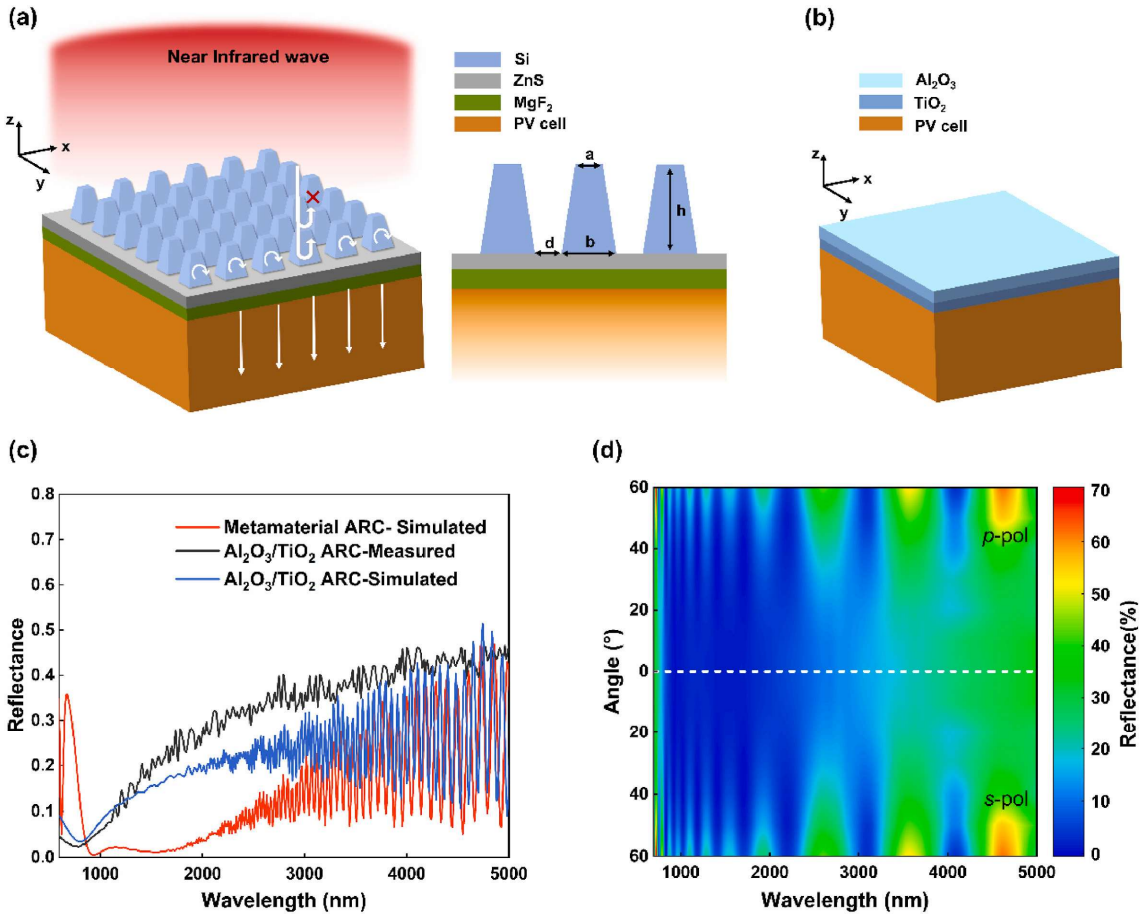

Figure 8. Schematic structures of (a) the designed metamaterial antireflective coating (ARC) and (b) the conventional Al_2O_3/TiO_2 ARC. (c) Variation in reflectance with wavelength for Al_2O_3/TiO_2 and metamaterial ARC. (d) Variation in metamaterial ARC with angle of incidence and wavelength (Reproduced from Ref. [172] with permission).

6.3. Multifunctional integration and real-time monitoring

Biometamaterials represent a novel class of applicators for microwave thermotherapy, offering improved uniformity in specific absorption rate (SAR) distributions. Incorporating metamaterials into microwave hyperthermia applicators enhances the precision and efficacy of targeted cancer treatment [173–175]. Electrically driven THz modulators based on active metamaterials improve spectroscopic imaging and phase-contrast detection [176]. Nonlinear metamaterials enable all-angle phase matching between counterpropagating modes, facilitating light localization and negative refraction, and providing a novel strategy for designing nonlinear lenses for high-resolution biphotonic microscopy of passive biological structures [177]. Porous CoCrMo implants with triply periodic minimal surface or rhombic dodecahedron architectures exhibit excellent mechanical properties and corrosion resistance, making them ideal for long-term implantation [178].

6.4. Sensing technologies

Biometamaterials provide remarkable versatility for physical and chemical sensing applications. Plasmonic metamaterial sensors enable ultrasensitive detection of biological and chemical targets [179,180], while complementary THz absorbers, with absorption rates reaching up to 97.3%, are effective for evaluating dielectric properties and material thickness [181].

6.5. Bone tissue engineering

The unique structural features and mechanical tunability of biometamaterials make them particularly suitable for bone tissue engineering. Auxetic structures (exhibiting negative Poisson's ratio) and porous elastic metamaterials are used to design orthopedic implants and scaffolds with enhanced load transfer and integration [4,9,157,162,182]. Additive manufacturing enables patient-specific implants tailored to anatomical geometries and mechanical properties [183–185]. Scaffolds made from CoCrMo alloys via laser powder bed fusion replicate bone-like elasticity and porosity [158].

6.6. Biometamaterials for cellular regulation and tissue regeneration

Biometamaterials play a vital role in controlling cellular behavior through microstructural design and surface modifications. Extrusion-based 3D printing techniques enable the fabrication of bio-instructive scaffolds with precise spatial and biochemical cues, offering controlled cellular guidance for tissue regeneration and highlighting future directions in metamaterials, hybrid living systems, and 4D printing [186], while dynamic, stimuli-responsive metamaterials mimic natural microenvironments to support tissue regeneration [187].

6.7. Mechanical optimization and fatigue performance

Optimizing the mechanical design and manufacturing processes of biometamaterials significantly enhances their fatigue performance, crucial for long-term biomedical applications. Studies have shown that structure, material selection, and post-processing strongly influence the fatigue life of metallic meta-biomaterials [10,154]. Daniel et al. [188] reported improvements in fatigue resistance through optimized 3D printing strategies. Sorrentino and Castagnetti [189] proposed a 3D rotating-tetrahedron auxetic metamaterial for bone replacement, while Zhao et al. [190] examined the dynamic compression response of Ti-6Al-4V multilayer micro-lattices. Kolken et al. [159] evaluated the fatigue behavior of auxetic implants, suggesting potential to reduce implant loosening.

6.8. Biocompatibility and surface modification

Surface treatments and functionalization are essential to improving biocompatibility. Graphene-integrated plasmonic sensors also enable tunable, high-sensitivity biosensing. A high-sensitivity plasmonic sensor based on a hexagonal nanorod array metasurface has been designed for distinguishing malignant hepatic metastases from healthy liver cells, offering nanoscale dimensions, tunable graphene integration, and angle-insensitive plasmon-induced absorption resonances [179].

3D-printed biometamaterials with bioinstructive design features, such as pore size, fiber orientation, and surface topography, can modulate cellular responses [186]. Kolken et al. [163] achieved decoupling of surface area and mechanical performance by hybridizing strut-lattice and minimal-surface topologies. Ganjian et al. [191] developed 3D biomaterials with tunable mechanical properties using nanopatterned metal sheets, and Wanniarachchi et al. [192] designed patient-specific CoCrMo scaffolds with high auxeticity for load-bearing bone regeneration.

Table 10. Comparative analysis: Biomedical applications.

Application/technique	Advantages	Disadvantages
Tissue engineering scaffolds (e.g., CoCrMo porous implants)	-Excellent mechanical strength and load-bearing capacity -High biocompatibility and corrosion resistance -Tunable porosity promotes osseointegration and vascularization	-Brittle nature and low ductility compared to natural tissue -Fabrication complexity with precise pore architecture - Potential long-term metal ion release
Acoustic/vibration sensors (e.g., piezoelectric metamaterial IR detectors)	-High sensitivity and real-time signal output -Capable of dual-function sensing and energy harvesting -Miniaturization compatible with wearable/implantable devices	-Limited material biocompatibility (e.g., lead-based piezoelectrics) -Performance degradation in moist or biological environments -Complex fabrication and packaging

Table 11. Comparative analysis: Surface modification techniques.

Technique	Advantages	Disadvantages
Graphene coating	-Excellent electrical and thermal conductivity enhancement. -High chemical and mechanical stability. -Effective as a barrier layer against oxidation or corrosion. -Biocompatible and promotes cell adhesion (in biomedical applications).	-Uniform, defect-free coating is difficult on large or complex surfaces. -Limited adhesion to some substrates without surface treatment. -High-quality synthesis (e.g., CVD graphene) can be costly.
Nanopatterning	-Allows precise control over surface topography at the nanoscale. -Enhances properties like wettability, adhesion, optical response, and cell behavior. -Suitable for tuning surface energy or mechanical interlocking.	-Often requires complex and expensive lithographic or etching techniques. -Scaling up for large-area applications is challenging. -Risk of structural instability under mechanical stress or high temperatures.

In addition, a substantial body of foundational and specialized reviews offers deeper insights into the development and applications of biometamaterials [153,157,183,184,188,193]. The approaches discussed in this section each present unique advantages and limitations. For the reader's convenience,

Tables 10 and 11 summarize a comparative analysis of these methods, highlighting their key strengths and current challenges.

7. Conclusions and future developments

In this review, I highlight the transformative potential of metamaterials in biomedicine, where their structural design capabilities allow for surpassing intrinsic limitations of conventional materials. Metamaterials are transitioning from proof-of-concept studies to practical biomedical solutions, with their advantages rooted in structural innovation, multifunctionality, and tunability. As intelligent manufacturing techniques advance, interdisciplinary collaboration deepens, and clinical translation mechanisms mature, metamaterials are poised to play a pivotal role in personalized medicine, precision diagnostics, and self-powered biomedical devices. Future innovations in materials science, fabrication technologies, and cross-disciplinary integration are expected to drive breakthroughs in smart healthcare, flexible electronics, and sustainable energy systems.

Despite significant progress, several challenges remain. Achieving an optimal balance between mechanical and biological functions is complex. While structural design can enhance mechanical properties, further research is needed to simultaneously fulfill biological requirements such as cell adhesion, vascularization, and tissue integration. For instance, although titanium-based auxetic materials enhance mechanical compliance, they remain susceptible to fatigue cracking under cyclic loading, highlighting the need for micro-damage modeling and structural optimization.

Sensor specificity and interference remain key technical hurdles. THz sensors, though highly sensitive, are vulnerable to water absorption and electromagnetic interference in physiological fluids. Additionally, challenges such as frequency band overlap in multi-analyte detection necessitate advanced structural design strategies.

In terms of biocompatibility and long-term stability, trade-offs between performance and safety persist. Piezoelectric ceramics offer high electromechanical coupling but often exhibit cytotoxicity and lack biodegradability. Conversely, piezoelectric polymers are more biocompatible but exhibit lower piezoelectric coefficients, which could be mitigated through composite formulations or nanoscale structuring.

Clinical translation is further impeded by the lack of standardized performance metrics, scalable production techniques, and long-term in vivo validation. Most work remains at the laboratory or animal model stage. Bridging this gap requires robust standardization, clinical protocols, and regulatory frameworks.

Looking ahead, the development of biomedical metamaterials will increasingly emphasize:

- Interdisciplinary integration and biomimetic design:

By combining biology, mechanics, and materials science, researchers can develop hierarchical metamaterials that mimic the multiscale architecture and functionality of natural tissues. For instance, spiderweb-inspired piezoelectric networks can significantly enhance energy harvesting performance.

- Intelligent response and dynamic regulation:

The integration of 4D printing and stimuli-responsive materials enables metamaterials to acquire dynamic functionalities, such as shape memory and controlled drug release, tailored to personalized medical needs.

• Green manufacturing and sustainability:

The development of bio-based piezoelectric materials, use of degradable polymers, and implementation of circular manufacturing strategies will contribute to environmentally friendly solutions in biomedical engineering.

• Clinical translation and standardization:

Establishing industry standards, strengthening academia-industry partnerships, and accelerating the path from lab-scale prototypes to clinical products are essential for widespread adoption.

Specific future research directions include:

1. Breakthroughs in biocompatible and degradable materials. Traditional piezoelectric materials (e.g., lead zirconate titanate, polyvinylidene fluoride) are limited by their rigidity and toxic elements. Emerging alternatives include natural and molecular ferroelectric materials (e.g., glycine, collagen, and molecular ferroelectric crystals like hexafluoropropylene-vinylidene fluoride copolymer), which combine high piezoelectric response with biocompatibility and biodegradability. For example, polyvinyl alcohol-based composites incorporating these materials have demonstrated piezoelectric coefficients as high as d_{33} = 10.4 pm/V and compatibility with dynamic physiological environments, making them suitable for drug delivery and regenerative medicine.

2. Nanostructuring and metamaterial design. Nanotechnology enables precise control of grain size and interface structures in piezoelectric materials, improving their processing, device performance, and mechanical flexibility. Electromechanical metamaterials, such as those developed by Dong Shuxiang's team, exploit symmetry-breaking designs to activate all 18 piezoelectric coefficients, enabling multifunctional devices for energy harvesting, sensing, and vibration control.

3. Lead-free and eco-friendly materials. Considering environmental regulations (e.g., European Union–Restriction of Hazardous Substances), the development of lead-free alternatives such as potassium sodium niobate (KNN) is gaining momentum. Continued improvement of their electromechanical performance and thermal stability is critical to their widespread adoption.

4. Implantable and transient medical devices. Emerging piezoelectric metamaterials (e.g., Ternary eutectic aqueous (TEA)-printed glycine/polyvinylpyrrolidone films) enable the development of flexible, biodegradable, and self-powered implants. These systems eliminate the need for surgical retrieval and support wireless energy harvesting (up to 35 $\mu W/cm^2$) via ultrasound, offering novel solutions for temporary or postoperative implants.

5. Smart sensing and tissue engineering. Biomimetic metamaterials that replicate the electromechanical properties of human skin or bone can enhance tissue regeneration. Combining piezoelectric activity with bioactive scaffolds enables the stimulation of cellular processes such as osteogenesis and neurogenesis.

6. Flexible electronics and wearable devices. Scalable techniques such as TEA printing enable the integration of piezoelectric films onto flexible substrates for wearable biosensors and energy harvesters. These systems are capable of powering small electronics through body motion and monitoring physiological signals (e.g., heart rate and respiration), with mechanical properties (e.g., Young's modulus of 180–440 MPa) optimized for comfort.

In summary, the convergence of advanced materials design, intelligent manufacturing, and clinical application is propelling biometamaterials toward transformative roles in next-generation medicine. Continued exploration and standardization efforts will be critical in realizing their full potential in diagnostics, therapeutics, and regenerative healthcare.

Use of AI tools declaration

The author declares that no artificial intelligence (AI) tools were used in the creation of this article.

Acknowledgments

The author is grateful for the financial support from National Natural Science Foundation of China (Grant No. 12272239), special projects in key fields of ordinary universities from Guangdong Provincial Department of Education (Grant No. 2022ZDZX3037), 2022 Stable Support Plan Program of Shenzhen Natural Science Fund.

Conflict of interest

Qing-Hua Qin is editor in chief for *AIMS Materials Science* and was not involved in the editorial review and the decision to publish this article. The author declares no conflict of interest.

References

1. Xiong C, Xiao Y, Qin QH (2025) Ultrawide bandgap optimization of porous 3D two-material phononic crystals aided by a 2D-based PnC construction method. *Model Simul Mater Sci Eng* 33: 015014. https://dx.doi.org/10.1088/1361-651X/ada174
2. Wang T, Sheng MP, Guo ZW, et al. (2016) Flexural wave suppression by an acoustic metamaterial plate. *Appl Acoust* 114: 118–124. https://doi.org/10.1016/j.apacoust.2016.07.023
3. Yin C, Xiao Y, Zhu D, et al. (2022) Design of low-frequency 1D phononic crystals harnessing compression–twist coupling effect with large deflection angle. *Thin Wall Struct* 179: 109600. https://doi.org/10.1016/j.tws.2022.109600
4. Shirzad M, Bodaghi M, Oh D, et al. (2024) Design and optimization of bioinspired auxetic structure for biomedical applications. *Eur J Mech A-Solids* 103: 105139. https://doi.org/10.1016/j.euromechsol.2023.105139
5. Xiong C, Xiao Y, Qin QH, et al. (2024) Bandgap design of 3D single-phase phononic crystals by geometric-constrained topology optimization. *AIMS Mater Sci* 11: 415–437. https://doi.org/10.3934/matersci.2024021
6. Dong J, Hu C, Holmes J, et al. (2022) Structural optimisation of cross-chiral metamaterial structures via genetic algorithm. *Compos Struct* 282: 115035. https://doi.org/10.1016/j.compstruct.2021.115035
7. Jiao P, Hasni H, Lajnef N, et al. (2020) Mechanical metamaterial piezoelectric nanogenerator (MM-PENG): Design principle, modeling and performance. *Mater Des* 187: 108214. https://doi.org/10.1016/j.matdes.2019.108214
8. Xu M, Zhao Z, Wang P, et al. (2022) Mechanical performance of bio-inspired hierarchical honeycomb metamaterials. *Int J Solids Struct* 254–255: 111866. https://doi.org/10.1016/j.ijsolstr.2022.111866
9. Clasky AJ, Watchorn JD, Chen PZ, et al. (2021) From prevention to diagnosis and treatment: Biomedical applications of metal nanoparticle-hydrogel composites. *Acta Biomater* 122: 1–25. https://doi.org/10.1016/j.actbio.2020.12.030

10. Huang H, Wang L, Fan Y (2023) Metallic meta-biomaterials: A critical review of fatigue behaviors. *J SCI-Adv Mater Dev* 8: 100585. https://doi.org/10.1016/j.jsamd.2023.100585
11. Shirzad M, Zolfagharian A, Bodaghi M, et al. (2023) Auxetic metamaterials for bone-implanted medical devices: Recent advances and new perspectives. *Eur J Mech A-Solids* 98: 104905. https://doi.org/10.1016/j.euromechsol.2022.104905
12. Cui N, Guan M, Xu M, et al. (2020) Design and application of terahertz metamaterial sensor based on DSRRs in clinical quantitative detection of carcinoembryonic antigen. *Opt Express* 28: 16834–16844. https://doi.org/10.1364/oe.393397
13. Wu J, Wang Z, Liang L, et al. (2025) Ultra-sensitive terahertz metamaterial sensors hybridized with graphene for trace detection of the cancer biomarker. *Opt Commun* 574: 131193. https://doi.org/10.1016/j.optcom.2024.131193
14. Keshavarz A, Vafapour Z (2019) Sensing avian influenza viruses using terahertz metamaterial reflector. *IEEE Sens J* 19: 5161–5166. https://doi.org/10.1109/JSEN.2019.2903731
15. Hu F, Guo E, Xu X, et al. (2017) Real-timely monitoring the interaction between bovine serum albumin and drugs in aqueous with terahertz metamaterial biosensor. *Opt Commun* 388: 62–67. https://doi.org/10.1016/j.optcom.2016.11.006
16. Tang H, Zhang S, Tian Y, et al. (2023) Bioinspired soft elastic metamaterials for reconstruction of natural hearing. *Adv Sci* 10: 2207273. https://doi.org/10.1002/advs.202207273
17. Li J, Yang F, Long Y, et al. (2021) Bulk ferroelectric metamaterial with enhanced piezoelectric and biomimetic mechanical properties from additive manufacturing. *ACS Nano* 15: 14903–14914. https://doi.org/10.1021/acsnano.1c05003
18. Wei J, Sun BH (2024) Study on the mechanical properties of cylindrical mechanical metamaterials with biomimetic honeycomb units of the diabolical ironclad beetle. *Extreme Mech Lett* 67: 102127. https://doi.org/10.1016/j.eml.2024.102127
19. Gao C, Li Y (2019) Mechanical model of bio-inspired composites with sutural tessellation. *J Mech Phys Solids* 122: 190–204. https://doi.org/10.1016/j.jmps.2018.09.015
20. Zhang Z, Song B, Fan J, et al. (2023) Design and 3D printing of graded bionic metamaterial inspired by pomelo peel for high energy absorption. *Chin J Mech Eng Addit Manuf Front* 2: 100068. https://doi.org/10.1016/j.cjmeam.2023.100068
21. Jiao P, Chen Z, Wang J (2024) Origami metamaterial biomimetic bouquets expand floriography to spatiotemporal 4D. *Cell Rep Phys Sci* 5: 101921. https://doi.org/10.1016/j.xcrp.2024.101921
22. Zhao Y, Wu Q, Zhao C, et al. (2024) Progress of structural scaffold biomaterials for bone tissue defect repair: A cutting-edge review. *Compos Struct* 349–350: 118542. https://doi.org/10.1016/j.compstruct.2024.118542
23. Tilton M, Borjali A, Isaacson A, et al. (2021) On structure and mechanics of biomimetic meta-biomaterials fabricated via metal additive manufacturing. *Mater Des* 201: 109498. https://doi.org/10.1016/j.matdes.2021.109498
24. Wei X, Ren C, Liu B, et al. (2025) The theory, technology, and application of terahertz metamaterial biosensors: A review. *Fundamental Res* 5: 571–585. https://doi.org/10.1016/j.fmre.2024.11.008
25. Wang W, Sun K, Xue Y, et al. (2024) A review of terahertz metamaterial sensors and their applications. *Opt Commun* 556: 130266. https://doi.org/10.1016/j.optcom.2024.130266

26. Pandey R, Kumar Mishra S, Kumar Dubey A (2024) Recent advances in smart piezoelectric biomaterials: Animal studies and beyond. *Chem Eng J* 500: 156750. https://doi.org/10.1016/j.cej.2024.156750
27. Yan Z, Tran H, Ma D, et al. (2024) Emerging piezoelectric metamaterials for biomedical applications. *Mater Interfaces* 1: 13–34. https://doi.org/10.53941/mi.2024.100004
28. Wang T, Wang H, Sheng MP, et al. (2016) Complete low-frequency bandgap in a two-dimensional phononic crystal with spindle-shaped inclusions. *Chin Phys B* 25: 046301. https://dx.doi.org/10.1088/1674-1056/25/4/046301
29. Hu C, Dong J, Luo J, et al. (2020) 3D printing of chiral carbon fiber reinforced polylactic acid composites with negative Poisson's ratios. *Compos Part B-Eng* 201: 108400. https://doi.org/10.1016/j.compositesb.2020.108400
30. Aghighi F, Morris J, Amirkhizi AV (2019) Low-frequency micro-structured mechanical metamaterials. *Mech Mater* 130: 65–75. https://doi.org/10.1016/j.mechmat.2018.12.008
31. Hussein MI, Leamy MJ, Ruzzene M (2014) Dynamics of phononic materials and structures: Historical origins, recent progress, and future outlook. *Appl Mech Rev* 66: 040802. https://doi.org/10.1115/1.4026911
32. Wang T, Sheng MP, Wang H, et al. (2015) Band structures in two-dimensional phononic crystals with periodic S-shaped slot. *Acoust Aust* 43: 275–281. https://doi.org/10.1007/s40857-015-0031-6
33. Fujita S, Ito K (2007) Bloch theorem, In: Fujita S, Ito K, *Quantum Theory of Conducting Matter: Newtonian Equations of Motion for a Bloch Electron*, New York, NY: Springer New York, 85–95. https://doi.org/10.1007/978-0-387-74103-1_7
34. Chen Z, Xia Y, He J, et al. (2020) Elastic-electro-mechanical modeling and analysis of piezoelectric metamaterial plate with a self-powered synchronized charge extraction circuit for vibration energy harvesting. *Mech Syst Signai Pr* 143: 106824. https://doi.org/10.1016/j.ymssp.2020.106824
35. Sugino C, Ruzzene M, Erturk A (2018) Design and analysis of piezoelectric metamaterial beams with synthetic impedance shunt circuits. *IEEE-ASME T Mech* 23: 2144–2155. http://dx.doi.org/10.1109/tmech.2018.2863257
36. Xu J, Yan R, Tang J (2018) Broadening bandgap width of piezoelectric metamaterial by introducing cavity. *Appl Sci* 8: 1606. https://doi.org/10.3390/app8091606
37. Gao W, Hu J, Qin Z, et al. (2023) Flexural wave manipulation in perforated metamaterial plates with acoustic black holes interconnected by piezoelectric studs. *Compos Struct* 321: 117224. https://doi.org/10.1016/j.compstruct.2023.117224
38. Pan W, Tang G, Tang J (2018) Evaluation of uncertainty effects to band gap behavior of circuitry-integrated piezoelectric metamaterial using order-reduced analysis. *J Intell Mater Syst Struct* 29: 2677–2692. https://journals.sagepub.com/doi/abs/10.1177/1045389X18778359
39. Xu J, Yan R (2018) Exploitation of dimension-dependent behavior of piezoelectric metamaterial with LC shunt circuit. *Eur Phys J Appl Phys* 83: 20501. https://doi.org/10.1051/epjap/2018180124
40. Sugino C, Ruzzene M, Erturk A (2020) Nonreciprocal piezoelectric metamaterial framework and circuit strategies. *Phys Rev B* 102: 014304. https://link.aps.org/doi/10.1103/PhysRevB.102.014304
41. Jiang R, Chen Y, Wang Z, et al. (2025) Modular bistable mechanical metamaterials: A versatile platform for piezoelectric self-charging, sensing, and logic operations. *Mater Today* 83: 96–112. https://doi.org/10.1016/j.mattod.2024.12.013

42. Yin P, Li B, Zhang Y, et al. (2025) A bioinspired multi-layer assembly method for mechanical metamaterials with extreme properties using topology optimization. *Comput Meth Appl Mech Eng* 438: 117850. https://doi.org/10.1016/j.cma.2025.117850
43. Yang J, Li Z, Xin X, et al. (2019) Designing electromechanical metamaterial with full nonzero piezoelectric coefficients. *Sci Adv* 5: eaax1782. https://doi.org/10.1126/sciadv.aax1782
44. Sugino C, Ruzzene M, Erturk A (2020) An analytical framework for locally resonant piezoelectric metamaterial plates. *Int J Solids Struct* 182–183: 281–294. https://doi.org/10.1016/j.ijsolstr.2019.08.011
45. Sugino C, Leadenham S, Ruzzene M, et al. (2017) Metamaterial piezoelectric beam with synthetic impedance shunts. *Proc SPIE* 2017: 1016410. https://doi.org/10.1117/12.2260320
46. Xu J, Tang J (2017) Tunable prism based on piezoelectric metamaterial for acoustic beam steering. *Appl Phys Lett* 110: 181902. https://doi.org/10.1063/1.4982717
47. Xu J, Tang J (2016) Acoustic prism for continuous beam steering based on piezo-electric metamaterial. *Proc SPIE* 2016: 97992I. https://doi.org/10.1117/12.2219464
48. Saadatzi M, Mir F, Saadatzi MN, et al. (2018) Modeling and fabrication of a multi-axial piezoelectric energy harvester based on a metamaterial-inspired structure. *IEEE Sens J* 18: 9410–9419. http://dx.doi.org/10.1109/JSEN.2018.2870993
49. Chen Z, He J, Wang G (2019) Vibration bandgaps of piezoelectric metamaterial plate with local resonators for vibration energy harvesting. *Shock Vib* 2019: 1397123. https://doi.org/10.1155/2019/1397123
50. Bao B, Lallart M, Guyomar D (2020) Manipulating elastic waves through piezoelectric metamaterial with nonlinear electrical switched dual-connected topologies. *Int J Mech Sci* 172: 105423. https://doi.org/10.1016/j.ijmecsci.2020.105423
51. Hu G, Tang L, Das R (2017) Metamaterial-inspired piezoelectric system with dual functionalities: Energy harvesting and vibration suppression. *Proc SPIE* 2017: 101641X. https://doi.org/10.1117/12.2260396
52. Kherraz N, Haumesser L, Levassort F, et al. (2018) Hybridization bandgap induced by an electrical resonance in piezoelectric metamaterial plates. *J Appl Phys* 123: 094901. https://doi.org/10.1063/1.5016496
53. Wang G, Cheng J, Chen J, et al. (2017) Multi-resonant piezoelectric shunting induced by digital controllers for subwavelength elastic wave attenuation in smart metamaterial. *Smart Mater Struct* 26: 025031. https://dx.doi.org/10.1088/1361-665X/aa53ea
54. Pan W, Tang G, Tang J (2017) Assessment of uncertainty effect in piezoelectric metamaterial. *Proc SPIE* 2017: 101650K. https://doi.org/10.1117/12.2260366
55. Li S, Xu J, Tang J (2017) Adaptive acoustic metamaterial with periodic piezoelectric network. *Proc SPIE* 2017: 101640N. https://doi.org/10.1117/12.2260333
56. Sun Y, Han Q, Jiang T, et al. (2024) Coupled bandgap properties and wave attenuation in the piezoelectric metamaterial beam on periodic elastic foundation. *Appl Math Model* 125: 293–310. https://doi.org/10.1016/j.apm.2023.09.030
57. Chen B, Zheng Y, Dai S, et al. (2024) Bandgap enhancement of a piezoelectric metamaterial beam shunted with circuits incorporating fractional and cubic nonlinearities. *Mech Syst Signai Pr* 212: 111262. https://doi.org/10.1016/j.ymssp.2024.111262
58. Hu G, Tang L, Das R, et al. (2018) Internally coupled piezoelectric metamaterial beam with multi-functionalities. *Proc SPIE* 2018: 1059516. https://doi.org/10.1117/12.2296451

59. Bao B, Guyomar D, Lallart M (2016) Electron–phonon metamaterial featuring nonlinear tri-interleaved piezoelectric topologies and its application in low-frequency vibration control. *Smart Mater Struct* 25: 095010. https://dx.doi.org/10.1088/0964-1726/25/9/095010
60. Jian Y, Hu G, Tang L, et al. (2023) Analytical and experimental study of a metamaterial beam with grading piezoelectric transducers for vibration attenuation band widening. *Eng Struct* 275: 115091. https://doi.org/10.1016/j.engstruct.2022.115091
61. Li Q, Wei B (2025) Vibration control of functionally graded composite annular plates reinforced with graphene origami-enabled auxetic metamaterials with piezoelectric layers. *Wave Motion* 136: 103539. https://doi.org/10.1016/j.wavemoti.2025.103539
62. Cai J, Yan L, Seyedkanani A, et al. (2024) Nano-architected GaN metamaterials with notable topology-dependent enhancement of piezoelectric energy harvesting. *Nano Energy* 129: 109990. https://doi.org/10.1016/j.nanoen.2024.109990
63. Xiao H, Li T, Zhang L, et al. (2023) Metamaterial based piezoelectric acoustic energy harvesting: Electromechanical coupled modeling and experimental validation. *Mech Syst Signai Pr* 185: 109808. https://doi.org/10.1016/j.ymssp.2022.109808
64. Huang W, Tang W, Chen Z, et al. (2025) Reinforcement-learning empowered adaptive piezoelectric metamaterial for variable-frequency vibration attenuation. *Eng Struct* 332: 120013. https://doi.org/10.1016/j.engstruct.2025.120013
65. Zhu X, Qiao J, Zhang G, et al. (2017) Tunable acoustic metamaterial based on piezoelectric ceramic transducer. *Proc SPIE* 2017: 1016411. https://doi.org/10.1117/12.2259963
66. Zhao JW, Yao LY, Zhang XD, et al. (2025) Investigation of elastic waves frequency converted for the piezoelectric metamaterial cylindrical shell. *Compos Struct* 354: 118799. https://doi.org/10.1016/j.compstruct.2024.118799
67. Rezaei S, Eskandari-Ghadi M, Rahimian M (2017) Simulation-based conceptual design of an acoustic metamaterial with full band gap using an air-based 1-3 piezoelectric composite for ultrasonic noise control. *Comptes Rendus Mécanique* 345: 137–152. https://doi.org/10.1016/j.crme.2016.11.003
68. Khan KA, Khan MA (2019) 3-3 Piezoelectric metamaterial with negative and zero Poisson's ratio for hydrophones applications. *Mater Res Bull* 112: 194–204. https://doi.org/10.1016/j.materresbull.2018.12.016
69. Xu J, Li S, Tang J (2017) Adaptive GRIN lens based on piezoelectric metamaterial for acoustic beam focusing. *Proc SPIE* 2017: 101641S. https://doi.org/10.1117/12.2260341
70. Wang M, Yi K, Zhu R (2023) Tunable underwater low-frequency sound absorption via locally resonant piezoelectric metamaterials. *J Sound Vibr* 548: 117514. https://doi.org/10.1016/j.jsv.2022.117514
71. Hui Y, Rinaldi M (2015) Spectrally selective infrared detector based on an ultra-thin piezoelectric resonant metamaterial. 2015 28th IEEE International Conference on Micro Electro Mechanical Systems (MEMS), Estoril, Portugal, 2015, 984–987. https://doi.org/10.1109/MEMSYS.2015.7051126
72. Wang C, Chen X, Song Q, et al. (2025) Investment micro-casting 3D-printed multi-metamaterial for programmable multimodal biomimetic electronics. *Device* 3: 100658. https://doi.org/10.1016/j.device.2024.100658

73. Annamdas VGM, Soh CK (2019) A perspective of non-fiber-optical metamaterial and piezoelectric material sensing in automated structural health monitoring. *Sensors-Basel* 19: 1490. https://doi.org/10.3390/s19071490
74. Kazim M, Pal A, Goswami D (2025) Mechanical metamaterials for bioengineering: In vitro, wearable, and implantable applications. *Adv Eng Mater* 27: 2401806. https://doi.org/10.1002/adem.202401806
75. Greco F, Codony D, Mohammadi H, et al. (2024) Topology optimization of flexoelectric metamaterials with apparent piezoelectricity. *J Mech Phys Solids* 183: 105477. https://doi.org/10.1016/j.jmps.2023.105477
76. Lin LF, Lu ZQ, Zhao L, et al. (2023) Vibration isolation of mechatronic metamaterial beam with resonant piezoelectric shunting. *Int J Mech Sci* 254: 108448. https://doi.org/10.1016/j.ijmecsci.2023.108448
77. Wang C, Zhao Z, Zhang XS (2023) Inverse design of magneto-active metasurfaces and robots: Theory, computation, and experimental validation. *Comput Meth Appl Mech Eng* 413: 116065. https://doi.org/10.1016/j.cma.2023.116065
78. Zhang Y, Jiang WZ, Zhang XY, et al. (2025) Re-entrant thermal-responsive metamaterials with widely tunable thermal expansion. *Compos Struct* 364: 119166. https://doi.org/10.1016/j.compstruct.2025.119166
79. Khalid MY, Arif ZU, Tariq A, et al. (2024) 3D printing of active mechanical metamaterials: A critical review. *Mater Des* 246: 113305. https://doi.org/10.1016/j.matdes.2024.113305
80. Hosseinkhani A, Rohan E (2024) Multi-functional periodically heterogeneous structures for energy harvesting and vibration attenuation-effects of piezoelectricity and shunting circuits. *Smart Mater Struct* 33: 115009. http://dx.doi.org/10.1088/1361-665X/ad7f33
81. Urban D (2025) Novel effects in light-actuated systems based on dispersed azobenzene dyes and azopolymers. PhD Thesis: NETU. Available from: https://hdl.handle.net/11250/3188965.
82. Zhang G, Xu C, Sun D, et al. (2025) Metasurface-tuned light-matter interactions for high-performance photodetectors. *Fundamental Res* (In press). https://doi.org/10.1016/j.fmre.2024.01.002
83. Gao Z, Lei Y, Li Z, et al. (2025) Artificial piezoelectric metamaterials. *Prog Mater Sci* 151: 101434. https://doi.org/10.1016/j.pmatsci.2025.101434
84. Ji G, Huber J (2022) Recent progress in acoustic metamaterials and active piezoelectric acoustic metamaterials—A review. *Appl Mater Today* 26: 101260. https://doi.org/10.1016/j.apmt.2021.101260
85. Ghafourivayghan M, Shabunin SN (2024) Feasibility assessment of guided resonance modes in high Q and resolution mm-wave metamaterial biosensor. *Optik* 299: 171619. https://doi.org/10.1016/j.ijleo.2024.171619
86. Le KQ, Bai J, Ngo QM, et al. (2017) Fabrication and numerical characterization of infrared metamaterial absorbers for refractometric biosensors. *J Electron Mater* 46: 668–6760 https://doi.org/10.1007/s11664-016-4979-2
87. Vafapour Z (2017) Near infrared biosensor based on classical electromagnetically induced reflectance (Cl-EIR) in a planar complementary metamaterial. *Opt Commun* 387: 1–11. https://doi.org/10.1016/j.optcom.2016.11.031

88. Fang J, Levchenko I, Yan W, et al. (2015) Plasmonic metamaterial sensor with ultra-high sensitivity in the visible spectral range. *Adv Opt Mater* 3: 750–755. https://doi.org/10.1002/adom.201400577
89. Liu Y, Ma WZ, Wu YC, et al. (2023) Multi-peak narrow-band metamaterial absorber for visible to near-infrared wavelengths. *Results Phys* 47: 106374. https://doi.org/10.1016/j.rinp.2023.106374
90. Danilov A, Tselikov G, Wu F, et al. (2018) Ultra-narrow surface lattice resonances in plasmonic metamaterial arrays for biosensing applications. *Biosens Bioelectron* 104: 102–112. https://doi.org/10.1016/j.bios.2017.12.001
91. Chen J, Hu F, Lin S, et al. (2024) Hybridization chain reaction assisted terahertz metamaterial biosensor for highly sensitive detection of microRNAs. *Spectrochim Acta A* 307: 123646. https://doi.org/10.1016/j.saa.2023.123646
92. Deng XS, Fang M, Ren, XG, et al. (2019) Ultra-sensitive bio-sensor based on trapped mode all-dielectric metasurface coating with graphene layer. *Acta Photonica Sinica* 48: 1248005. http://dx.doi.org/10.3788/gzxb20194812.1248005
93. Bi H, You R, Bian X, et al. (2024) A magnetic control enrichment technique combined with terahertz metamaterial biosensor for detecting SARS-CoV-2 spike protein. *Biosens Bioelectron* 243: 115763. https://doi.org/10.1016/j.bios.2023.115763
94. Kazemi F, Tabatabaeian ZS, Zarrabi FB (2024) A terahertz metamaterial biosensor based on spoof surface plasmon polaritons transmission line for avian influenza virus detection. *Opt Laser Technol* 174: 110694. https://doi.org/10.1016/j.optlastec.2024.110694
95. Li Y, Chen X, Hu F, et al. (2019) Four resonators based high sensitive terahertz metamaterial biosensor used for measuring concentration of protein. *J Phys D Appl Phys* 52: 095105. https://dx.doi.org/10.1088/1361-6463/aaf7e9
96. Luigi La S, Filiberto B, Lucio V (2011) Metamaterial resonator arrays for organic and inorganic compound sensing. *Proc SPIE* 2011: 83060I. https://doi.org/10.1117/12.912267
97. Tripathy SK, Gorai A, Behera TM, et al. (2024) A miniaturized dual band terahertz metamaterial based absorber as a biosensor for non-melanoma skin cancer diognostic. *Optik* 316: 172048. https://doi.org/10.1016/j.ijleo.2024.172048
98. Zhang C, Liang L, Ding L, et al. (2016) Label-free measurements on cell apoptosis using a terahertz metamaterial-based biosensor. *Appl Phys Lett* 108: 241105. https://doi.org/10.1063/1.4954015
99. Zhang Z, Yang M, Liang L, et al. (2019) Biosensor platforms of the polarization-dependent metamaterials for the detection of cancer-cell concentration. *Proc SPIE* 2019: 111960X. https://doi.org/10.1117/12.2534423
100. Yang M, Zhang Z, Yan X, et al. (2019) The biosensing of liver cancer cells based on the terahertz plasmonic metamaterials *Proc SPIE* 2019: 111960E. https://doi.org/10.1117/12.2536419
101. Keshavarz A, Vafapour Z (2019) Water-based terahertz metamaterial for skin cancer detection application. *IEEE Sens J* 19: 1519–1524. https://doi.org/10.1109/JSEN.2018.2882363
102. Haque SMA, Ahmed M, Alqahtani A, et al. (2024) Modelling and analysis of a triple-band metamaterial absorber for early-stage cervical cancer HeLa cell detection. *Opt Lasers Eng* 181: 108426. https://doi.org/10.1016/j.optlaseng.2024.108426

103. Mahfuz T, Hossan A, Rahman N (2025) Design of a polarization independent terahertz metamaterial absorber for biomedical sensing applications. *Biosens Bioelectron:X* 22: 100560. https://doi.org/10.1016/j.biosx.2024.100560
104. Kim M, Kang DH, Choi JH, et al. (2024) Highly sensitive and label-free protein immunoassay-based biosensor comprising infrared metamaterial absorber inducing strong coupling. *Biosens Bioelectron* 260: 116436. https://doi.org/10.1016/j.bios.2024.116436
105. Kim T, Kwak J, Roh Y, et al. (2025) Terahertz metamaterial on-chip sensing platform for live cancer cell microenvironment analysis. *Chem Eng J* 509: 161370. https://doi.org/10.1016/j.cej.2025.161370
106. Upender P, Kumar A (2025) Numerical investigation of a high-performance MXene and graphene-based metamaterial absorber for terahertz biosensing. *Results Phys* 70: 108185. https://doi.org/10.1016/j.rinp.2025.108185
107. Shakiba L, Salehi MR, Emami F (2024) A multiband perfect metamaterial absorber based on phase change material for switching and biosensing applications. *Opt Commun* 560: 130498. https://doi.org/10.1016/j.optcom.2024.130498
108. Yang M, Zhang Z, Liang L, et al. (2019) Sensitive detection of the concentrations for normal epithelial cells based on Fano resonance metamaterial biosensors in terahertz range. *Appl Optics* 58: 6268–6273. https://doi.org/10.1364/AO.58.006268
109. Yu W, Li J, Huang G, et al. (2024) Rapid and sensitive detection of Staphylococcus aureus using a THz metamaterial biosensor based on aptamer-functionalized Fe_3O_4@Au nanocomposites. *Talanta* 272: 125760. https://doi.org/10.1016/j.talanta.2024.125760
110. Chen K, Ruan C, Zhan F, et al. (2023) Ultra-sensitive terahertz metamaterials biosensor based on luxuriant gaps structure. *iScience* 26: 105781. https://doi.org/10.1016/j.isci.2022.105781
111. Yang K, Li J, Lamy de la Chapelle M, et al. (2021) A terahertz metamaterial biosensor for sensitive detection of microRNAs based on gold-nanoparticles and strand displacement amplification. *Biosens Bioelectron* 175: 112874. https://doi.org/10.1016/j.bios.2020.112874
112. Prajapati YK, Pal S, Saini JP (2018) Effect of a metamaterial and silicon layers on performance of surface plasmon resonance biosensor in infrared range. *Silicon-Neth* 10: 1451–1460. https://doi.org/10.1007/s12633-017-9625-y
113. Mirzaei S, Green NG, Rotaru M, et al. (2017) Detecting and identifying DNA via the THz backbone frequency using a metamaterial-based label-free biosensor. *Proc SPIE* 2017: 101031I. https://doi.org/10.1117/12.2263694
114. Zhao L, Niu Q, He Z, et al. (2018) Theoretical excitation of 2-D (1, 1) cavity mode with asymmetric sword-shaped notched square resonators for metamaterial perfect multiband absorbers in infrared range. *Opt Express* 26: 31510–31522. https://doi.org/10.1364/OE.26.031510
115. Zhao R, Zou B, Zhang G, et al. (2020) High-sensitivity identification of aflatoxin B1 and B2 using terahertz time-domain spectroscopy and metamaterial-based terahertz biosensor. *J Phys D: Appl Phys* 53: 195401. https://dx.doi.org/10.1088/1361-6463/ab6f90
116. Wu X, Quan B, Pan X, et al. (2013) Alkanethiol-functionalized terahertz metamaterial as label-free, highly-sensitive and specific biosensor. *Biosens Bioelectron* 42: 626–631. https://doi.org/10.1016/j.bios.2012.10.095
117. Tang M, Xia L, Wei D, et al. (2020) Rapid and label-free metamaterial-based biosensor for fatty acid detection with terahertz time-domain spectroscopy. *Spectrochim Acta A* 228: 117736. https://doi.org/10.1016/j.saa.2019.117736

118. Wang H, Cai J, Wang T, et al. (2024) Functionalized gold nanoparticle enhanced nanorod hyperbolic metamaterial biosensor for highly sensitive detection of carcinoembryonic antigen. *Biosens Bioelectron* 257: 116295. https://doi.org/10.1016/j.bios.2024.116295
119. Geng Z, Zhang X, Fan Z, et al. (2017) A route to terahertz metamaterial biosensor integrated with microfluidics for liver cancer biomarker testing in early stage. *Sci Rep* 7: 16378. https://doi.org/10.1038/s41598-017-16762-y
120. Xu W, Xie L, Zhu J, et al. (2019) Terahertz biosensing with a graphene-metamaterial heterostructure platform. *Carbon* 141: 247–252. https://doi.org/10.1016/j.carbon.2018.09.050
121. Zhang R, Chen Q, Liu K, et al. (2019) Terahertz microfluidic metamaterial biosensor for sensitive detection of small-volume liquid samples. *IEEE Trans Terahertz Sci Technol* 9: 209–214. https://doi.org/10.1109/TTHZ.2019.2898390
122. Sugumaran S, Jamlos MF, Ahmad MN, et al. (2018) Nanostructured materials with plasmonic nanobiosensors for early cancer detection: A past and future prospect. *Biosens Bioelectron* 100: 361–373. https://doi.org/10.1016/j.bios.2017.08.044
123. Salim A, Lim S (2018) Review of recent metamaterial microfluidic sensors. *Sensors-Basel* 18: 232. https://doi.org/10.3390/s18010232
124. Shamim S, Mohsin ASM, Rahman MM, et al. (2024) Recent advances in the metamaterial and metasurface-based biosensor in the gigahertz, terahertz, and optical frequency domains. *Heliyon* 10: e33272. https://doi.org/10.1016/j.heliyon.2024.e33272
125. RoyChoudhury S, Rawat V, Jalal AH, et al. (2016) Recent advances in metamaterial split-ring-resonator circuits as biosensors and therapeutic agents. *Biosens Bioelectron* 86: 595–608. https://doi.org/10.1016/j.bios.2016.07.020
126. Hassan MM, Sium FS, Islam F, et al. (2021) A review on plasmonic and metamaterial based biosensing platforms for virus detection. *Sens Bio-Sens Res* 33: 100429. https://doi.org/10.1016/j.sbsr.2021.100429
127. Verma A, Yadav BC (2024) Comprehensive review on two dimensional nanomaterials for optical biosensors: Present progress and outlook. *Sustain Mater Techno* 40: e00900. https://doi.org/10.1016/j.susmat.2024.e00900
128. Liu J, Fan L, Su J, et al. (2022) Study on a terahertz biosensor based on graphene-metamaterial. *Spectrochim Acta A* 280: 121527. https://doi.org/10.1016/j.saa.2022.121527
129. Tewatia A, Pal S, Pal N (2018) Performance evaluation of surface plasmon resonance biosensor using metamaterial. *Mater Today Proc* 5: 28384–28391. https://doi.org/10.1016/j.matpr.2018.10.123
130. Nishino T, Tanigawa H, Sekiguchi A (2018) Antifouling technology of metamaterial structure using biomimetic technology. *Proc SPIE* 2018: 1072804. https://doi.org/10.1117/12.2320471
131. Nishino T, Tanigawa H, Sekiguchi A (2018) Antifouling effect on biomimetic metamaterial surfaces. *J Photopolym Sci Tec* 31: 129–132. https://doi.org/10.2494/photopolymer.31.129
132. Khoshhesab MM, Li Y (2018) Mechanical behavior of 3D printed biomimetic Koch fractal contact and interlocking. *Extreme Mech Lett* 24: 58–65. https://doi.org/10.1016/j.eml.2018.09.003
133. Jiang Y, Li Y (2018) 3D printed auxetic mechanical metamaterial with chiral cells and re-entrant cores. *Sci Rep* 8: 2397. https://doi.org/10.1038/s41598-018-20795-2
134. Jiang Y, Li Y (2018) Novel 3D-printed hybrid auxetic mechanical metamaterial with chirality-induced sequential cell opening mechanisms. *Adv Eng Mater* 20: 1700744. https://doi.org/10.1002/adem.201700744

135. Yang N, Silverberg JL (2017) Decoupling local mechanics from large-scale structure in modular metamaterials. *PNAS* 114: 3590–3595. https://doi.org/10.1073/pnas.1620714114
136. Wang H, Zhao J, Wang X, et al. (2025) Multi-functional metamaterial based on overdamping effect: Design, investigation, optimization. *Int J Mech Sci* 286: 109890. https://doi.org/10.1016/j.ijmecsci.2024.109890
137. Zeng Q, Zhao Z, Lei H, et al. (2023) A deep learning approach for inverse design of gradient mechanical metamaterials. *Int J Mech Sci* 240: 107920. https://doi.org/10.1016/j.ijmecsci.2022.107920
138. Chang T, Jeon S, Heo M, et al. (2020) Mimicking bio-mechanical principles in photonic metamaterials for giant broadband nonlinearity. *Commun Phys* 3: 79. https://doi.org/10.1038/s42005-020-0352-0
139. Chen Y, Ai B, Wong ZJ (2020) Soft optical metamaterials. *Nano Converg* 7: 18. https://doi.org/10.1186/s40580-020-00226-7
140. Duan Y, Xia C, Chen W, et al. (2025) A bio-inspired broadband absorption metamaterial: Driven by dual-structure synergistically induced current vortices. *J Mater Sci Technol* 206: 193–201. https://doi.org/10.1016/j.jmst.2024.03.053
141. Li G, Tan L, Ren L, et al. (2023) Biomimetic 4D printing of dome-shaped dynamic mechanical metamaterials. *J Mater Res Technol* 24: 4047–4059. https://doi.org/10.1016/j.jmrt.2023.04.039
142. Silva B, Govan J, Cristóbal Zagal J, et al. (2023) A biomimetic smart kirigami soft metamaterial with multimodal remote locomotion mechanisms. *Mater Des* 233: 112262. https://doi.org/10.1016/j.matdes.2023.112262
143. Liu L, Li Y (2018) Failure mechanism transition of 3D-printed biomimetic sutures. *Eng Fract Mech* 199: 372–379. https://doi.org/10.1016/j.engfracmech.2018.06.013
144. Jackson JA, Messner MC, Dudukovic NA, et al. (2018) Field responsive mechanical metamaterials. *Sci Adv* 4: eaau6419. https://doi.org/10.1126/sciadv.aau6419
145. Badloe T, Kim I, Rho J (2020) Biomimetic ultra-broadband perfect absorbers optimised with reinforcement learning. *Phys Chem Chem Phys* 22: 2337–2342. https://doi.org/10.1039/C9CP05621A
146. She W, Wu Z, Yang J, et al. (2024) Cement-based biomimetic metamaterials. *J Build Eng* 94: 110050. https://doi.org/10.1016/j.jobe.2024.110050
147. Ignuta-Ciuncanu MC, Tabor P, Martinez-Botas RF (2024) A generative design framework for passive thermal control with macroscopic metamaterials. *Therm Sci Eng Prog* 51: 102637. https://doi.org/10.1016/j.tsep.2024.102637
148. Vangelatos Z, Yildizdag ME, Grigoropoulos CP (2023) A designer's challenge: Unraveling the architected structure of deep sea sponges for lattice mechanical metamaterials. *Extreme Mech Lett* 61: 102013. https://doi.org/10.1016/j.eml.2023.102013
149. Song B, Zhang L, Shi Y (2023) Chapter 5—Biological metamaterials, In: Song B, Zhao A, Zhang L, et al. *Metamaterial Design and Additive Manufacturing*, New York: Academic Press, 139–221. https://doi.org/10.1016/B978-0-443-18900-5.00005-8
150. Wang C, Lu X, Yang X, et al. (2025) Biomimetic Kagome-Gyroid interpenetrating metamaterial for tailoring lightweight and mechanical performance. *Mater Des* 252: 113729. https://doi.org/10.1016/j.matdes.2025.113729

151. De Maio U, Greco F, Fabbrocino F, et al. (2024) Structural stability investigation in bioinspired metamaterials based on glass sponge microstructures. *Procedia Struct Integrity* 66: 502–510. https://doi.org/10.1016/j.prostr.2024.11.103
152. Gaetano D, Greco F, Leonetti L, et al. (2025) Instability issues in microstructured solids embedding cohesive and contact interfaces. *Prog Eng Sci* 2: 100082. https://doi.org/10.1016/j.pes.2025.100082
153. Zadpoor AA (2019) Mechanical performance of additively manufactured meta-biomaterials. *Acta Biomater* 85: 41–59. https://doi.org/10.1016/j.actbio.2018.12.038
154. Kolken HMA, Garcia AF, Plessis AD, et al. (2022) Mechanisms of fatigue crack initiation and propagation in auxetic meta-biomaterials. *Acta Biomater* 138: 398–409. https://doi.org/10.1016/j.actbio.2021.11.002
155. Ma T, Huang Q, He H, et al. (2019) All-dielectric metamaterial analogue of electromagnetically induced transparency and its sensing application in terahertz range. *Opt Express* 27: 16624–16634. https://doi.org/10.1364/OE.27.016624
156. Novin SN, Zarrabi FB, Bazgir M, et al. (2019) Field enhancement in metamaterial split ring resonator aperture nano-antenna with spherical nano-particle arrangement. *Silicon* 11: 293–300. https://doi.org/10.1007/s12633-018-9854-8
157. Jiang D, Thissen H, Hughes TC, et al. (2024) Advances in additive manufacturing of auxetic structures for biomedical applications. *Mater Today Commun* 40: 110045. https://doi.org/10.1016/j.mtcomm.2024.110045
158. Wanniarachchi CT, Arjunan A, Baroutaji A, et al. (2023) 3D printing customised stiffness-matched meta-biomaterial with near-zero auxeticity for load-bearing tissue repair. *Bioprinting* 33: e00292. https://doi.org/10.1016/j.bprint.2023.e00292
159. Kolken HMA, Garcia AF, Du Plessis A, et al. (2021) Fatigue performance of auxetic meta-biomaterials. *Acta Biomater* 126: 511–523. https://doi.org/10.1016/j.actbio.2021.03.015
160. Gric T, Sokolovski SG, Navolokin N, et al. (2020) Metamaterial formalism approach for advancing the recognition of glioma areas in brain tissue biopsies. *Opt Mater Express* 10: 1607–1615. https://doi.org/10.1364/OME.393604
161. Naify CJ, Rohde CA, Martin TP, et al. (2016) Generation of topologically diverse acoustic vortex beams using a compact metamaterial aperture. *Appl Phys Lett* 108: 223503. https://doi.org/10.1063/1.4953075
162. Wanniarachchi CT, Arjunan A, Baroutaji A, et al. (2022) Mechanical performance of additively manufactured cobalt-chromium-molybdenum auxetic meta-biomaterial bone scaffolds. *J Mech Behav Biomed Mater* 134: 105409. https://doi.org/10.1016/j.jmbbm.2022.105409
163. Kolken HMA, Callens SJP, Leeflang MA, et al. (2022) Merging strut-based and minimal surface meta-biomaterials: Decoupling surface area from mechanical properties. *Addit Manuf* 52: 102684. https://doi.org/10.1016/j.addma.2022.102684
164. De Maio U, Greco F, Nevone Blasi P, et al. (2024) Elastic wave propagation control in porous and finitely deformed locally resonant nacre-like metamaterials. *Materials* 17: 705. https://doi.org/10.3390/ma17030705
165. Bollineni RK, Ahmed MS, Shahab S, et al. (2024) Nacre-like block lattice metamaterials with targeted phononic band gap and mechanical properties. *J Mech Behav Biomed Mater* 154: 106511. https://doi.org/10.1016/j.jmbbm.2024.106511

166. Pranno A, Greco F, Leonetti L, et al. (2022) Band gap tuning through microscopic instabilities of compressively loaded lightened nacre-like composite metamaterials. *Compos Struct* 282: 115032. https://doi.org/10.1016/j.compstruct.2021.115032
167. Huang XT, Lu CH, Rong CC, et al. (2018) Wide angle of incidence-insensitive polarization-independent THz metamaterial absorber for both TE and TM mode based on plasmon hybridizations. *Materials* 11: 671. https://doi.org/10.3390/ma11050671
168. Xia L, Cui HL, Zhang M, et al. (2019) Broadband anisotropy in terahertz metamaterial with single-layer gap ring array. *Materials* 12: 2255. https://doi.org/10.3390/ma12142255
169. Chen Y, Yang X, Tong W, et al. (2019) The simulation on absorption properties of metamaterial/GaAs/electrode layer hybrid structure based Terahertz photoconductive detector. *Opt Mater Express* 51: 118. https://doi.org/10.1007/s11082-019-1834-8
170. Zhu W, Rukhlenko ID, Xiao F, et al. (2014) Polarization conversion in U-shaped chiral metamaterial with four-fold symmetry breaking. *J Appl Phys* 115: 143101. https://doi.org/10.1063/1.4870862
171. Zhu W, Rukhlenko ID, Premaratne M (2013) Graphene metamaterial for optical reflection modulation. *Appl Phys Lett* 102: 241914. https://doi.org/10.1063/1.4812200
172. Yi Y, Xu Z, Cai T, et al. (2025) Antireflective all-dielectric metamaterials for thermophotovoltaic systems based on multiresonance. *Opt Commun* 574: 131229. https://doi.org/10.1016/j.optcom.2024.131229
173. Khuyen BX, Hanh VTH, Tung BS, et al. (2020) Narrow/broad-band absorption based on water-hybrid metamaterial. *Crystals* 10: 415. https://doi.org/10.3390/cryst10050415
174. Vrba D, Vrba J (2014) Applicators for local microwave hyperthermia based on metamaterial technology. The 8th European Conference on Antennas and Propagation (EuCAP 2014), The Hague, Netherlands, 68–71. https://doi.org/10.1109/EuCAP.2014.6901694
175. Vrba D, Vrba J (2014) Novel applicators for local microwave hyperthermia based on zeroth-order mode resonator metamaterial. *Int J Antennas Propag* 2014: 631398. https://doi.org/10.1155/2014/631398
176. Peralta XG, Wanke MC, Brener I, et al. (2010) Metamaterial based devices for terahertz imaging. *Proc SPIE* 2010: 75620I. https://doi.org/10.1117/12.846823
177. Ciracì C, Centeno E (2009) Focusing of second-harmonic signals with nonlinear metamaterial lenses: A biphotonic microscopy approach. *Phys Rev Lett* 103: 063901. https://doi.org/10.1103/PhysRevLett.103.063901
178. Munyensanga P, Bricha M, El Mabrouk K (2024) Functional characterization of biomechanical loading and biocorrosion resistance properties of novel additively manufactured porous CoCrMo implant: Comparative analysis with gyroid and rhombic dodecahedron. *Mater Chem Phys* 316: 129139. https://doi.org/10.1016/j.matchemphys.2024.129139
179. Rakhshani MR (2021) Wide-angle perfect absorber using a 3D nanorod metasurface as a plasmonic sensor for detecting cancerous cells and its tuning with a graphene layer. *Photonic Nanostruct* 43: 100883. https://doi.org/10.1016/j.photonics.2020.100883
180. Hwang I, Yu J, Lee J, et al. (2018) Plasmon-enhanced infrared spectroscopy based on metamaterial absorbers with dielectric nanopedestals. *ACS Photonics* 5: 3492–3498. https://doi.org/10.1021/acsphotonics.8b00702

181. Faruk A, Sabah C (2019) Absorber and sensor applications of complimentary H-shaped fishnet metamaterial for sub-terahertz frequency region. *Optik* 177: 64–70. https://doi.org/10.1016/j.ijleo.2018.09.145
182. Zhang L, Wang B, Song B, et al. (2023) 3D printed biomimetic metamaterials with graded porosity and tapering topology for improved cell seeding and bone regeneration. *Bioact Mater* 25: 677–688. https://doi.org/10.1016/j.bioactmat.2022.07.009
183. Vyavahare S, Mahesh V, Mahesh V, et al. (2023) Additively manufactured meta-biomaterials: A state-of-the-art review. *Compos Struct* 305: 116491. https://doi.org/10.1016/j.compstruct.2022.116491
184. Dogan E, Bhusal A, Cecen B, et al. (2020) 3D printing metamaterials towards tissue engineering. *Appl Mater Today* 20: 100752. https://doi.org/10.1016/j.apmt.2020.100752
185. Jia Z, Xu X, Zhu D, et al. (2023) Design, printing, and engineering of regenerative biomaterials for personalized bone healthcare. *Prog Mater Sci* 134: 101072. https://doi.org/10.1016/j.pmatsci.2023.101072
186. Zieliński PS, Gudeti PKR, Rikmanspoel T, et al. (2023) 3D printing of bio-instructive materials: Toward directing the cell. *Bioact Mater* 19: 292–327. https://doi.org/10.1016/j.bioactmat.2022.04.008
187. Wu DJ, Bouten CVC, Dankers PYW (2017) From molecular design to 3D printed life-like materials with unprecedented properties. *Curr Opin Biomed Eng* 2: 43–48. https://doi.org/10.1016/j.cobme.2017.06.001
188. Daniel A, Bakhtiari H, Nouri A, et al. (2025) Fatigue properties of 3D-printed polymeric metamaterials: A review. *SMMF* 3: 100076. https://doi.org/10.1016/j.smmf.2025.100076
189. Sorrentino A, Castagnetti D (2024) Periodic tetrahedral auxetic metamaterial. *Extreme Mech Lett* 71: 102214. https://doi.org/10.1016/j.eml.2024.102214
190. Zhao Y, Wu Q, Zhou H, et al. (2024) Investigation on mechanical properties of Ti-6Al-4 V multilayer micro-lattice biomaterials under dynamic compression loading. *J Alloy Compd* 977: 173419. https://doi.org/10.1016/j.jallcom.2024.173419
191. Ganjian M, Janbaz S, van Manen T, et al. (2022) Controlled metal crumpling as an alternative to folding for the fabrication of nanopatterned meta-biomaterials. *Mater Des* 220: 110844. https://doi.org/10.1016/j.matdes.2022.110844
192. Wanniarachchi CT, Arjunan A, Baroutaji A, et al. (2024) 3D printed CoCrMo personalised load-bearing meta-scaffold for critical size tibial reconstruction. *Ann 3D Print Med* 15: 100163. https://doi.org/10.1016/j.stlm.2024.100163
193. Wang C, Vangelatos Z, Grigoropoulos CP, et al. (2022) Micro-engineered architected metamaterials for cell and tissue engineering. *Mater Today Adv* 13: 100206. https://doi.org/10.1016/j.mtadv.2022.100206

AIMS Press